NATIONAL AERONAUTICS AND SPACE ADMINISTRATION

TECHNICAL REPORT
R-26

SKIN-FRICTION MEASUREMENTS IN INCOMPRESSIBLE FLOW

By DONALD W. SMITH and JOHN H. WALKER

1959

TECHNICAL REPORT R-26

SKIN-FRICTION MEASUREMENTS IN INCOMPRESSIBLE FLOW

FLOW

By DONALD W. SMITH and JOHN H. WALKER

Ames Research Center
Moffett Field, Calif.

TECHNICAL REPORT R-26

SKIN-FRICTION MEASUREMENTS IN INCOMPRESSIBLE FLOW [1]

By Donald W. Smith and John H. Walker

SUMMARY

Experiments have been conducted to measure in incompressible flow the local surface-shear stress and the average skin-friction coefficient for a turbulent boundary layer on a smooth, flat plate having zero pressure gradient. The local surface-shear stress was measured by a floating-element skin-friction balance and also by a calibrated total head tube located on the surface of the test wall. The average skin-friction coefficient was obtained from boundary-layer velocity profiles. The boundary-layer profiles were also used to determine the location of the virtual origin of the turbulent boundary layer. Data were obtained for a range of Reynolds numbers from 1 million to about 45 million with an attendant change in Mach number from 0.11 to 0.32.

The measured local skin-friction coefficients obtained with the floating-element balance agree well with those of Schultz-Grunow and Kempf for Reynolds numbers up to 45 million. The measured average skin-friction coefficients agree with those given by the Schoenherr curve in the ranges of Reynolds numbers from 1 to 3 million and 30 to 45 million. In the range of Reynolds numbers from 3 to 30 million the measured values are less than those predicted by the Schoenherr curve.

The results show that the "universal skin-friction constants" proposed by Coles approach asymptotically a constant value at Reynolds numbers exceeding 21 million. Because of the scatter in the aforementioned constants and the limited Reynolds number range of the present investigation, there is some doubt as to the validity of any turbulent skin-friction law written on the basis of the present results. Hence, no new friction law is proposed.

The frictional resistance of a flat plate was calculated by means of the momentum method and

also the integrated measured local surface shear. For Reynolds numbers from 14 million to 45 million both methods give about the same result; whereas at lower values of Reynolds number the momentum method based on velocity profiles uncorrected for the effects of turbulence results in a frictional resistance as much as 4 percent higher than that of the integrated shear.

The measurement of local surface shear by a calibrated Preston tube appears to be accurate and inexpensive. The calibration as given by Preston must be modified slightly, however, to yield the results obtained from the floating-element skin-friction balance.

INTRODUCTION

In recent years there has been a resurgence of interest in the problem of the turbulent boundary layer on a smooth flat plate having zero pressure gradient along its length or breadth. This interest falls into two categories. First, it is necessary for the aeronautical designer to know the effect of Reynolds number variation on the average skin-friction coefficient for the accurate prediction of both drag and heat transfer. Secondly, there has been considerable controversy in England among hydrodynamicists with regard to the variation of average skin-friction coefficient with changing Reynolds number (see refs. 1 through 4) and hence the ability to project ship-model test results to full-scale Reynolds numbers.

Up to this time much work has been done in attempts to determine a so-called skin-friction law for incompressible fluids. Most of this work has been experimental in nature, leading to a law having empirically determined constants.

It was intended in the present work to determine accurately the empirical constants required to write a skin-friction law by making use of the

[1] Supersedes NACA Technical Note 4231 by Donald W. Smith and John H. Walker.

1

modern techniques now available for measuring local surface-shear stress and by use of extremely accurate manometers for measuring the local velocity in the boundary layer. By the use of such techniques, it was hoped that a friction law could be determined with an accuracy of ± 2 percent particularly for large Reynolds numbers. The investigation also included an evaluation of the accuracy of a method, proposed by Preston in reference 5, involving the use of a single surface tube to determine local surface-shear stress.

NOTATION

C_f	local skin-friction coefficient, $\dfrac{\tau_w}{q}$
C_F	average skin-friction coefficient, $\dfrac{2\theta}{x}$
C_p	pressure coefficient, $\dfrac{p-p_\infty}{q_\infty}$, dimensionless
C_1	constant in skin-friction equation, $\dfrac{V\delta^*}{u^*\delta}$
C_2	constant in skin-friction equation, $\left(\dfrac{V}{u^*}\right)^2\dfrac{\delta^*-\theta}{\delta}$
d	inside diameter, in.
D	outside diameter, in.
H	shape parameter, $\dfrac{\delta^*}{\theta}$
k	slope of wall law and velocity-defect law curves in the similarity region
M	Mach number
p	local static pressure, lb/sq in.
p_∞	free-stream static pressure, lb/sq in.
p_t	local total pressure, lb/sq in.
p_{t_∞}	free-stream total pressure, lb/sq in.
q_∞	free-stream dynamic pressure, lb/sq in.
R_x	Reynolds number, $\dfrac{Vx}{\nu}$
R_θ	Reynolds number, $\dfrac{V\theta}{\nu}$
T	temperature, °F
u	local velocity, ft/sec
u^*	friction velocity, $\sqrt{\dfrac{\tau_w}{\rho}}$, ft/sec
V	free-stream velocity, ft/sec
w_{trip}	weight flow of air ejected from boundary-layer trip, lb/sec
x	distance in the direction of flow from the virtual origin of the turbulent boundary layer, in.

y	vertical distance from wall, in.
z	spanwise distance across channel, measured from center line of channel, in.
δ	boundary-layer thickness, y at $\dfrac{u}{V}=0.990$, in.
δ^*	boundary-layer displacement thickness, $\delta\int_0^1\left(1-\dfrac{\rho u}{\rho_\infty V}\right)d\left(\dfrac{y}{\delta}\right)$, in.
θ	boundary-layer momentum thickness, $\delta\int_0^1\dfrac{\rho u}{\rho_\infty V}\left(1-\dfrac{u}{V}\right)d\left(\dfrac{y}{\delta}\right)$, in.
μ	absolute viscosity, lb sec/sq ft
ν	kinematic viscosity, sq ft/sec
ρ	local density, lb sec^2/ft^4
ρ_∞	free-stream density, lb sec^2/ft^4
τ_w	surface friction stress, lb/sq ft
$\phi(0)$	$\dfrac{u}{u^*}$ when $\dfrac{yu^*}{\nu}=1.0$ or when $\log_{10}\dfrac{yu^*}{\nu}=0$ (See fig. 15(a).)
$\phi(1)-\phi(0)$	$\dfrac{V-u}{u^*}$ when $\dfrac{yu^*}{\delta^*V}=\dfrac{1}{C_1}$ (See fig. 15(b).)

EQUIPMENT

MODEL

The friction measurements were made on a flat plate which formed one wall of a channel mounted in the wind tunnel as shown in figure 1. The test wall was mounted between a pair of end plates to which was attached an adjustable auxiliary plate approximately parallel to the test wall. The auxiliary plate could be adjusted to change the longitudinal pressure gradient in the
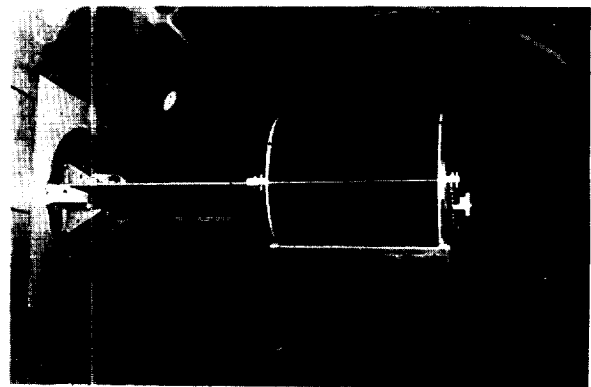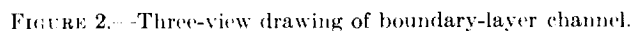

A–21103

FIGURE 1.—Boundary-layer channel in the test section of the Ames 12-foot pressure wind tunnel.

Note: All dimensions shown in inches

Figure 2.—Three-view drawing of boundary-layer channel.

channel. Preliminary measurements indicated that without the auxiliary plate the longitudinal pressure gradient along the test wall was not uniform.

The test wall of the channel and the auxiliary wall opposite were identical in cross section. The nose was elliptical with a ratio of major axis to minor axis of 2.0. The trailing edge was sharp, having a circular-arc section tangent to the surface 3 inches forward of the trailing edge (fig. 2). The test wall was made of mild steel polished to a fine finish. Measurements with an interferometer indicated that, generally, the test wall had a surface finish of 20 to 40 microinches (peak to valley). There were a few streamwise scratches on the surface which were deeper than this but it is believed that they had little or no effect on the flow.

The other three walls of the channel were made of aluminum and had a finish about equal to that of the test wall. All holes and joints were sealed to prevent the flow of air from the higher pressure stream of the tunnel into the channel at other than the front opening.

A permanent boundary-layer trip was installed near the leading edge of the test wall (fig. 3). This trip was of the air ejection type used by

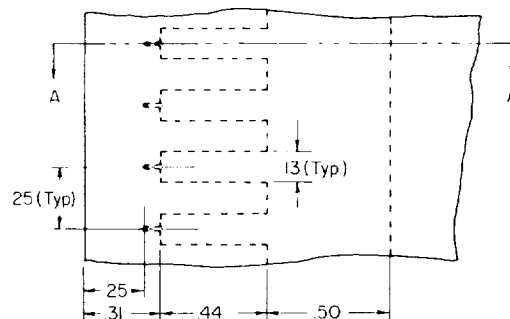Section A-A

Note: All dimensions shown in inches

Figure 3.—Details of boundary-layer trip.

Fage and Sargent (ref. 6). The trip will be discussed further in the section on test conditions.

WIND TUNNEL

This experimental investigation was done in the Ames 12-foot pressure wind tunnel. The wind tunnel is of the variable-density type providing Reynolds numbers up to 10 million per foot at a Mach number of about 0.30 and Reynolds numbers up to 1.7 million per foot at Mach numbers up to about 0.95. The turbulence level of the wind-tunnel air stream is very low.

EXPERIMENTAL METHODS

The reliability of skin-friction measurements is critically dependent upon the precision of the measuring apparatus. It, therefore, seems appropriate to discuss in some detail the characteristics of the measuring apparatus, the degree of precision attained, and the procedure used in conducting the tests.

LOCAL VELOCITY MEASUREMENTS

The velocity profiles through the boundary layer were determined from measurements with a total-pressure tube and a static-pressure orifice in the plate, located at the same longitudinal station. The total-pressure tube was very carefully constructed with a flattened end which was 0.007-inch high and 0.080-inch wide. The wall thickness was 0.002 inch. (See fig. 4.) The opening of the tube was perpendicular to the direction of the free stream and was free of burrs and imperfections. This tube was mounted on a screw device which allowed it to be moved perpendicular to the wall. This screw was calibrated and found to be capable

of positioning the tube to 0.001 inch. The zero position of the tube was determined by an electrical circuit which was energized when the total-head tube made contact with the plate. This method was quite successful and was found to be capable of consistently indicating the zero position to 0.001 inch. This accuracy was only possible if the wall and tube were kept scrupulously clean and free of all oxides, oil, and foreign matter.

The quantities measured were the local total pressure in the boundary layer, the static pressure at the wall, and the vertical distance from the surface of the wall to the center line of the face of the total-pressure tube. It was assumed that the static pressure was constant through the boundary layer and that the total temperature in the boundary layer was equal to the total temperature in the tunnel settling chamber. Because of the small vertical dimension of the total-pressure tube, no correction was applied to the measured height of the tube above the test wall to account for the apparent displacement of the tube resulting from the total-pressure gradient through the boundary layer. No correction was applied to the velocity profiles for the effect of turbulence.

An additional probe was constructed for use in the determination of the location of boundary-layer transition. The longitudinal variation of the surface velocity near the leading edge of the plate was measured. This device was capable of traversing the plate in a streamwise direction from 0.5 inch aft of the leading edge to about 3.25 inches aft of the leading edge. The local total pressure was measured with a probe having the same dimensions as the one previously described (see fig. 4) and the static pressure was measured with a 0.035-inch-diameter static-pressure probe located 1.0 inch away from the surface of the plate and at the same longitudinal station as the total-pressure probe. Local velocities were computed from these measurements using the same assumptions as were made for the surveys through the boundary layer.

LOCAL SURFACE-SHEAR MEASUREMENT

The local surface-shear stress was measured by two different techniques. The first of these made use of a floating-element device which measured the shear stress directly. The second technique made use of a calibrated total-pressure tube mounted on the surface of the wall as proposed by J. H. Preston. Preston made measurements with
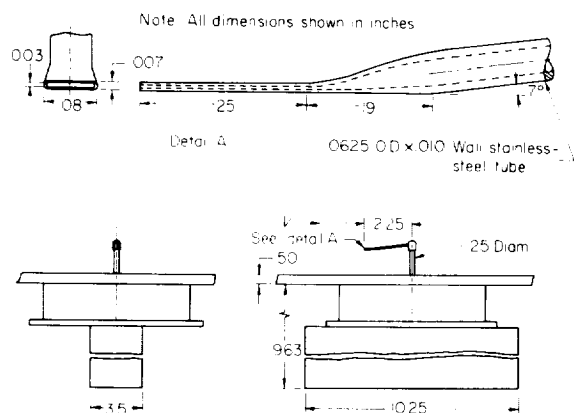

Note All dimensions shown in inches

003   007
08   25   9

Detail A

0625 O.D × .010 Wall stainless-steel tube

See Detail A   225   25 Diam
50
963
35   1025

FIGURE 4.—Details of velocity probe and probe mounting mechanism.

air flow in a pipe, whereas the present measurements with surface tubes were made to validate and determine the accuracy of the technique for air flow on a flat plate and to verify Preston's calibration of the tubes.

Floating-element device.—The local surface-shear stress was measured by a floating-element-type device similar to that used by Dhawan (ref. 7) and others. The floating-element technique was also used by Schultz-Grunow (ref. 8) and Kempf (ref. 9) in their historically important surface-shear measurements.

Since little is known about the effect of change of the size of gap around the floating element on the measured surface shear, it was decided to construct a device whose element could be repositioned and centered in the gap. Both Schultz-Grunow and Kempf used such a device while Dhawan and others used a simple deflection-type instrument. In the present unit the floating element was repositioned by a small, powerful electromagnet. The position of the element was indicated by a differential transformer capable of indicating movement of the floating element to an accuracy of a few millionths of an inch. When the position indicator showed that the floating element had started to move from its no-load neutral position, the strength of the electromagnet was varied until the element returned to its no-load neutral position. Since the electromagnetic force was equal and opposite to the drag force exerted on the element, the average surface-shear stress on the floating element could be deduced from the measured electromagnetic force and a predetermined calibration.
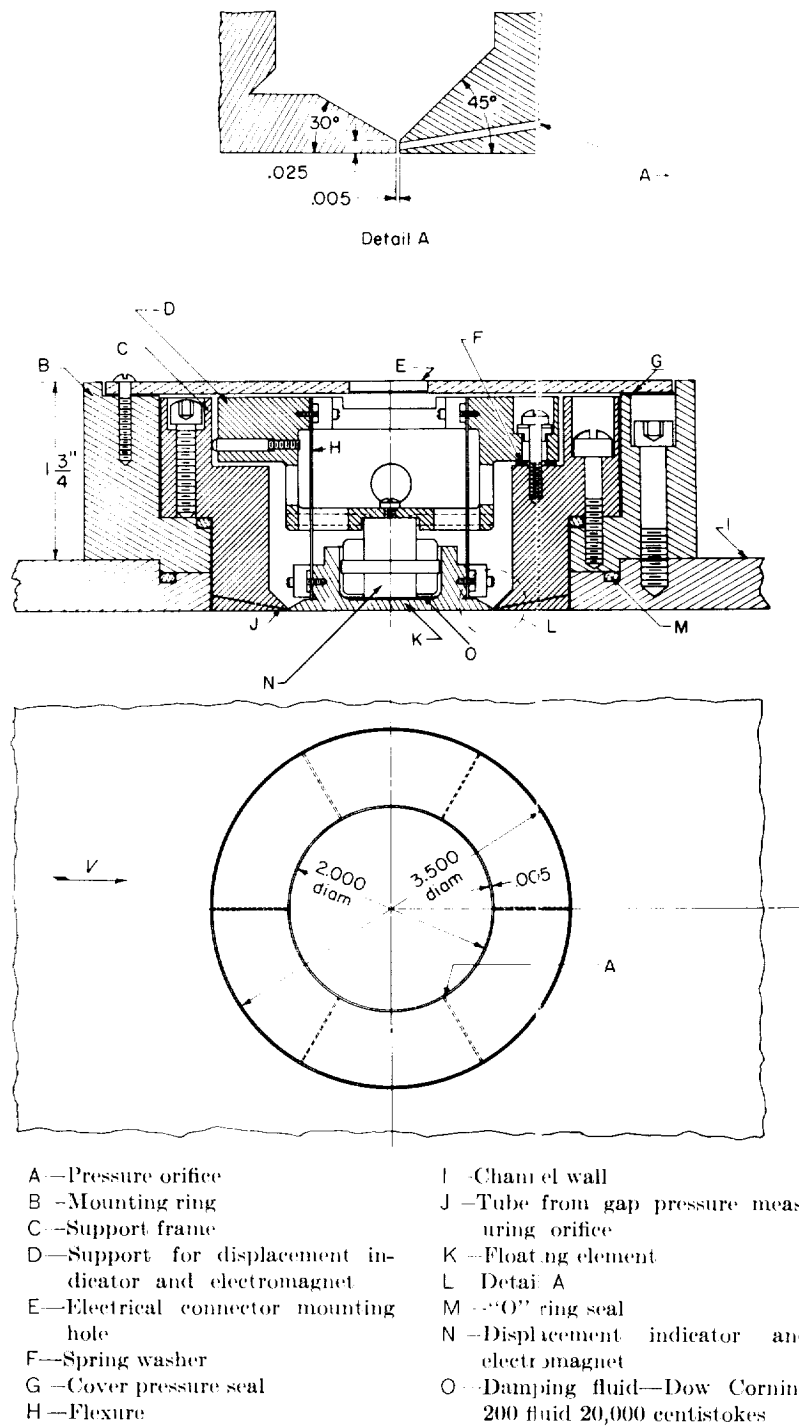
The shear-stress measuring device was capable of indicating the drag force on the element with a sensitivity of about 0.02×10^{-3} pounds for a range of force from 0 to about 30×10^{-3} pounds. The accuracy of determining the load under test conditions is believed to be within ± 2 percent of applied load throughout the load range encountered in the tests. Calibrations of the element displayed extremely good repeatability. The measured data were corrected for effects of change in temperature of the unit.

In figure 5 is presented a detailed drawing of the shear-stress measuring device. This device consisted of a 2-inch-diameter plate which was mounted on very limber flexure pivots. The flexure pivots were, in turn, attached to a sturdy support frame which was mounted on the working wall of the boundary-layer channel. As may be seen in figure 5, the support frame and movable plate were mounted on the channel wall in an integral unit. The 2-inch-diameter movable plate was centered in a 2.010-inch-diameter hole in the support frame with its working surface set flush with the working surface of the support frame. The surface of the floating-element unit was carefully alined flush with the surface of the channel wall using both dial and interferometric indicators. It was possible to position the element surface within about ± 0.00005 inch by means of the dial indicator.

Tests were made to study the effects of small variations in flushness of the floating element with the surrounding fixed surface. Measurements of surface shear at identical test conditions were made for a range of positions of the floating element, both depressed below and protruding above the fixed surface of the plate. It was found that the surface of the floating element could be depressed as much as 0.0005 inch without any change in the surface shear. However, when the element protruded above the surface of the wall, there were noticeable deviations in the measured shear force. Consequently, the surface element was always maintained flush with or slightly below the surface of the channel wall.

The entire floating-element unit was constructed of Invar in order to minimize the effect of temperature changes on the calibration of the unit. The faces of both the support frame and the floating plate were very carefully lapped to ensure both a fine surface finish and also flat surfaces having sharp edges on the inside and outside diameters of the units. Interferometric measurements indicated that the surface had a peak-to-valley roughness of about 10 to 20 microinches and a flatness of about 20 to 40 microinches. The floating-element unit was made into a pressure-tight capsule to prevent the flow of high-pressure air from the tunnel main flow into the higher speed flow of the boundary-layer channel. Damping of the floating element was achieved by using 20,000 centistoke oil in a cup machined integral with the back of the element. The cup was adjusted to have 0.005-inch clearance with the displacement indicator and electromagnet which are fixed to the support frame (see fig. 5).

Detail A

A—Pressure orifice
B—Mounting ring
C—Support frame
D—Support for displacement indicator and electromagnet
E—Electrical connector mounting hole
F—Spring washer
G—Cover pressure seal
H—Flexure

I—Channel wall
J—Tube from gap pressure measuring orifice
K—Floating element
L—Detail A
M—"O" ring seal
N—Displacement indicator and electromagnet
O—Damping fluid—Dow Corning 200 fluid 20,000 centistokes

FIGURE 5.—Details of the floating-element skin-friction balance.

The static pressure in the gap between the float-ing element and the channel wall was measured by means of six static orifices in the gap (see fig. 5) and a buoyancy correction was applied to the surface-shear force measured on the element. This correction was always less than 1 percent of the applied force on the element.

Surface-tube shear-stress device.—In 1953 a very simple technique for measuring surface-shear stress was proposed by J. H. Preston (see ref. 5). This technique made use of the total pressure measured by a round total-head tube mounted flush with the surface (see fig. 6). The pressure measured by the total-head tube in conjunction with the surface static pressure measured at the same location along the plate was calibrated by Preston in terms of the local surface-shear stress.

Two total-head tubes having outside diameters of 0.0300 inch and 0.1217 inch, respectively, were

Tube 1: $d=.0180$ $D=.0300$
Tube 2: $d=.0730$ $D=.1217$

Detail A

.062 Diam. static pressure orifice

3.50 Diam.

Note: All dimensions are shown in inches

See detail A

.125 Diam. tube

1.75

.50

6.00 Diam.

Section A-A

FIGURE 6.—Details of the Preston surface-shear tubes.

used in the present investigation. The tubes had a ratio of inside diameter to outside diameter of 0.600, the same proportions used by Preston. Care was taken to make the mouth of the tube perpendicular to the longitudinal axis of the tube. The equations and assumptions used in the reduc-tion of the measured data are given in reference 5.

SENSITIVE MANOMETER

In order to measure the velocities in the bound-ary layer and the pressures associated with the surface-tube shear-stress device with sufficient ac-curacy to give an over-all accuracy of results of 1 percent or better, it was necessary to devise a manometer capable of measuring very small pres-sure differences over a large range of pressure difference. Such a device was designed and built and was found to be capable of indicating a pres-sure difference of about 0.06 pound per square foot with an accuracy of ±0.12 pound per square foot for pressure differences as large as 600 pounds per square foot.

This manometer was of the U-tube type with a float in the low-pressure leg of the system. This float had a steel slug incorporated in it and a servo-operated follower mounted on a lead screw alongside the manometer leg to indicate the posi-tion of the slug in the leg of the manometer. The lead screw was calibrated in terms of the pressure difference applied across the two legs of the ma-nometer. The glass tubes used in this manometer were precision bored to have an inside diameter of 0.750 ±0.001 inch. The fluid (tetrabromo-ethane) in the manometer was maintained at a fixed temperature of 107° F ±½° F.

The bore of each manometer tube was coated with Dri Film, a General Electric silicone product, to reduce the effect of the meniscus of the fluid on the pressure readings. Calculations show that the capillary effect of the meniscus could result in a maximum error of about 0.2 pound per square foot in the pressure reading if the angle of con-tact between the manometer fluid and the glass tube varied from 0° to 90°. Because of the Dri Film coating it is felt that the error in measured pressure due to capillary forces has been reduced to a value considerably smaller than the accuracy of the indicating system of the manometer.

Due to the fact that this instrument had a large range of indication and extremely high sensitivity, the calibration of the instrument posed some dif-
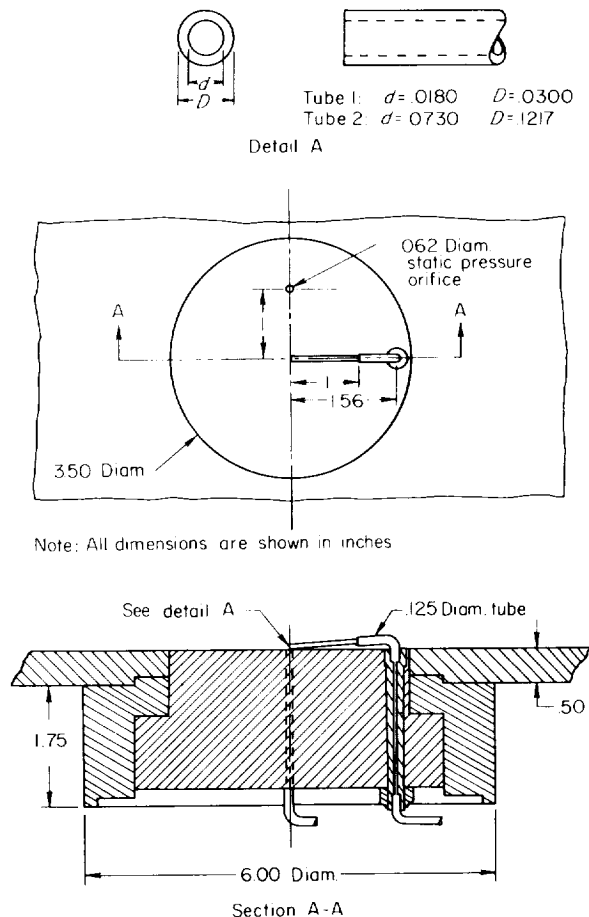
ficulty. Since there was no instrument available to use as a standard, it was decided to determine the specific gravity of the fluid at the stabilized temperature (107° F) and use this as the calibration of the instrument in conjunction with an accurate calibration of the lead screw follower.

TEST CONDITIONS

The Reynolds number in the present tests varied from about 1 million to 10 million per foot of channel length. This range of Reynolds numbers was obtained by varying the tunnel total pressure from 8 to 80 pounds per square inch absolute and the Mach number from 0.11 to 0.32. These values of Mach number are in the range where compressibility effects in the air flow are generally considered insignificant.

VELOCITY PROFILES

The boundary-layer velocity profiles were measured at stations 1.312, 2.312, 3.312, and 4.312 feet aft of the leading edge of the channel wall. The most forward measurement station (0.312 feet aft of leading edge) was not used since the velocity profiles were distorted and were of no interest. The longitudinal locations used provided Reynolds numbers based on the distance

from the leading edge from about 1 million to about 43 million.

SURFACE-SHEAR STRESS

Local surface-shear stress was measured at stations 1.5, 2.5, 3.5, and 4.5 feet aft of the leading edge of the channel wall as is shown in figure 2. Again the most forward measuring station (0.5 feet aft of the leading edge) was not used because of the distorted velocity profiles. The Reynolds number based on the distance of these stations from the leading edge varied from about 1.5 million to 45 million.

LONGITUDINAL PRESSURE GRADIENT

The longitudinal static-pressure gradient measured on the test surface of the boundary-layer channel is presented in figure 7. At the leading edge of the channel there was a pressure peak which is not shown in the figure. Throughout the major portion of the channel, where measurements were made, the local static pressure varied less than about 0.5 percent of the velocity head from the reference static pressure at the longitudinal midpoint of the channel. As may be seen in figure 7 there was little effect of change in either Mach number or tunnel total pressure on the pressure gradient.
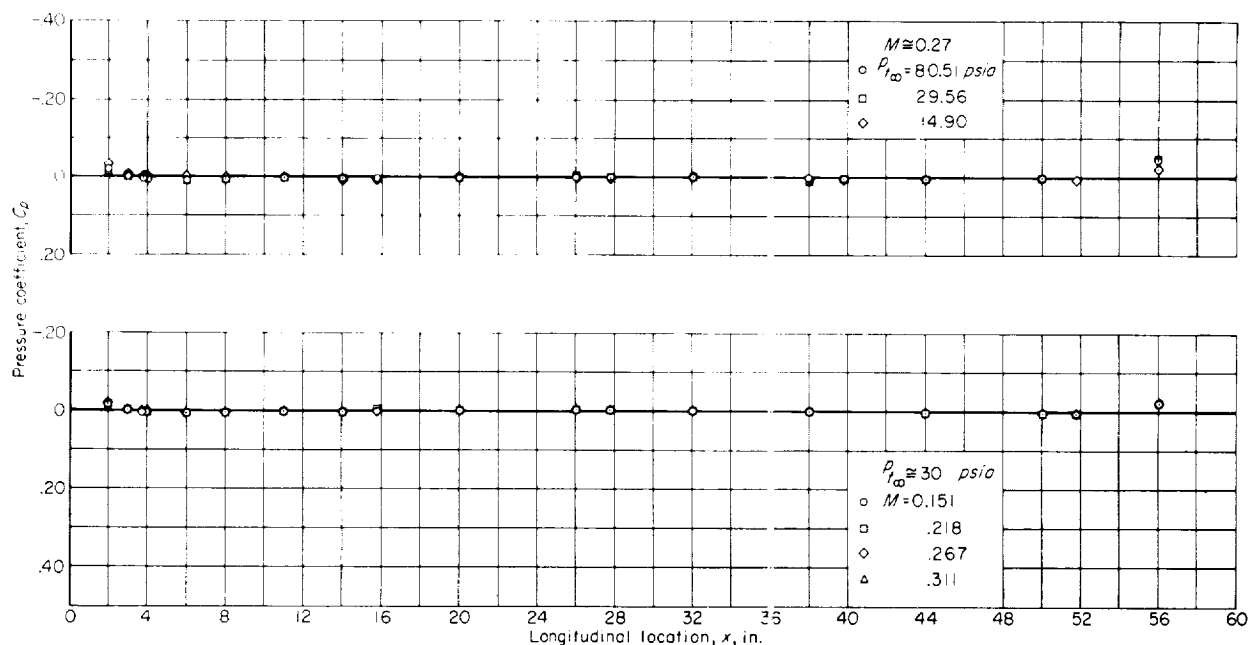

FIGURE 7.—Longitudinal pressure gradient in boundary-layer channel.

BOUNDARY-LAYER TRIP

A boundary-layer trip was provided to assure a two-dimensional turbulent boundary layer near the leading edge of the working wall of the channel. An air-injection-type trip was chosen because it could be readily varied in strength to trip the boundary layer with the least amount of disturbance. The geometry of the trip is given in figure 3.

The quantity of air to be ejected from the trip was determined using longitudinal velocity surveys which were made at the surface of the plate with a total-pressure and a static-pressure tube. Typical longitudinal velocity distributions at the plate surface for various amounts of ejected air are presented in figure 8. When no air was ejected
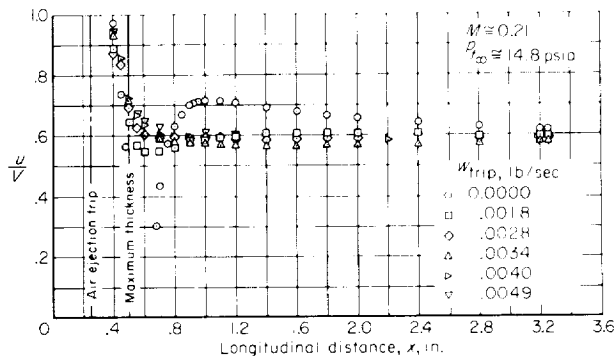

FIGURE 8.—Effect of varying quantity of boundary-layer-trip air on local velocity near channel wall.

from the trip, it appeared that some type of separation phenomenon was present. However, when air was ejected from the trip, this phenomenon disappeared and it seemed that the boundary layer became turbulent within about 0.25 inch of the trip. It was not possible to keep the probe on the surface of the wall forward of the maximum-thickness point and therefore the data forward of this point do not represent surface measurements.

For the Mach number and total-pressure condition in figure 8, the air quantity selected as that which assured a turbulent boundary layer with the least distortion was 0.0034 pound per second. A similar set of surveys was made for each test condition and the air quantities selected in this manner were utilized for their particular test conditions.

TWO-DIMENSIONALITY OF FLOW

As was previously mentioned the walls of the channel were capable of being moved with respect

to one another to provide for adjustment of the longitudinal static-pressure gradient. These walls were also adjusted so that the static pressure did not vary in the transverse direction.

To check the two-dimensionality of the flow, boundary-layer velocity profiles were measured at three spanwise locations at the same longitudinal station. The spanwise locations chosen for the measurements were at the center line of the working wall of the channel and at 7 inches either side of the center line. These three profiles for several test conditions are presented in figure 9. Their
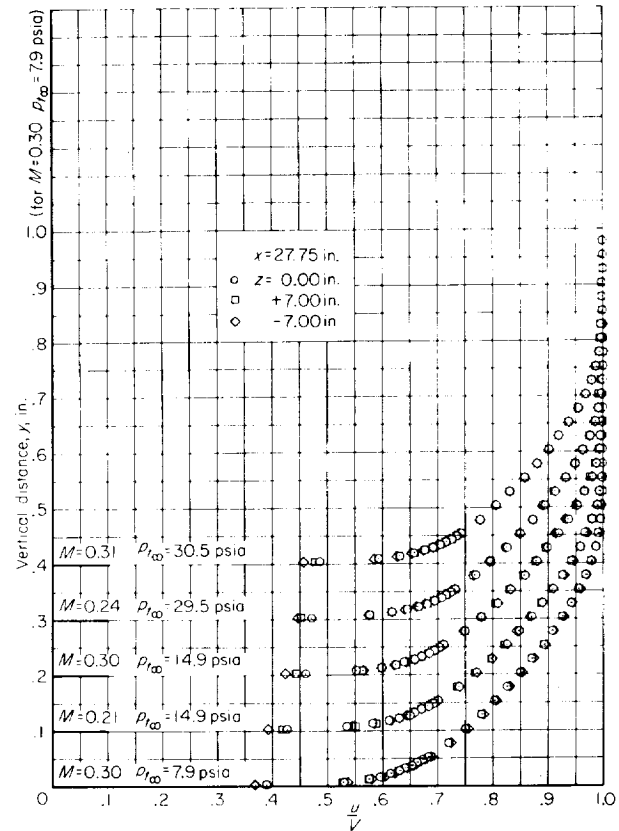

FIGURE 9.—Effect of spanwise location in boundary-layer channel on velocity profile.

similarity indicates a flow which closely approximates two-dimensional flow.

DETERMINATION OF VIRTUAL ORIGIN OF TURBULENCE

Physically, the turbulent boundary layer can not start with zero thickness and the virtual origin of the turbulent layer must therefore be estimated. One simple method for making such an estimate

was proposed by Rubesin, et al. (ref. 10), and this method has been used in the present report.

The virtual origin of turbulence was estimated by plotting log 2θ versus log x (where x is the distance from the leading edge of the test surface) and determining the magnitude of the change in x required to make the slope of the line equal to some reference value.

The reference value of the slope, d (log 2θ)/ d (log x), which was used was the mean value of the slopes computed for each of four logarithmic laws presented in reference 11. (The law by Schultz-Grunow was omitted.) The reference value of slope used for the estimation of the virtual origin varied from about 0.826 to 0.850 for a variation of Reynolds number per foot from about 1 million to 10 million.

It was found that for all conditions at which tests were made, the change in x was within ± 1 inch and in many cases was within $\pm\frac{1}{2}$ inch. On the basis of this analysis and due to the fact that the results scattered on both sides of zero, it was concluded that the leading edge of the working wall of the channel could be used as the virtual origin of the turbulent boundary layer and the distance from the leading edge to the point of measurement could be used as the reference distance for Reynolds number.

PRESENTATION AND DISCUSSION OF RESULTS

The principal results of the investigation are presented in tables I, II, and III. Table I contains measured velocity profile data for all test conditions. Table II contains the measured values of local skin-friction coefficient as a function of Reynolds number. In table III is presented a summary of the major boundary-layer parameters obtained from the boundary-layer velocity profiles.

There are presented in figure 10 some of the velocity profiles tabulated in table I. These profiles are typical of the profiles obtained for all test conditions. All of the measured velocity profiles have been mechanically integrated to obtain both the boundary-layer displacement thickness, δ^*, and momentum thickness, θ. The ratio of these two parameters, known as the shape parameter, H, has been computed and tabulated in table III. These results are presented in figure 11 as a function of the Reynolds number. As was expected
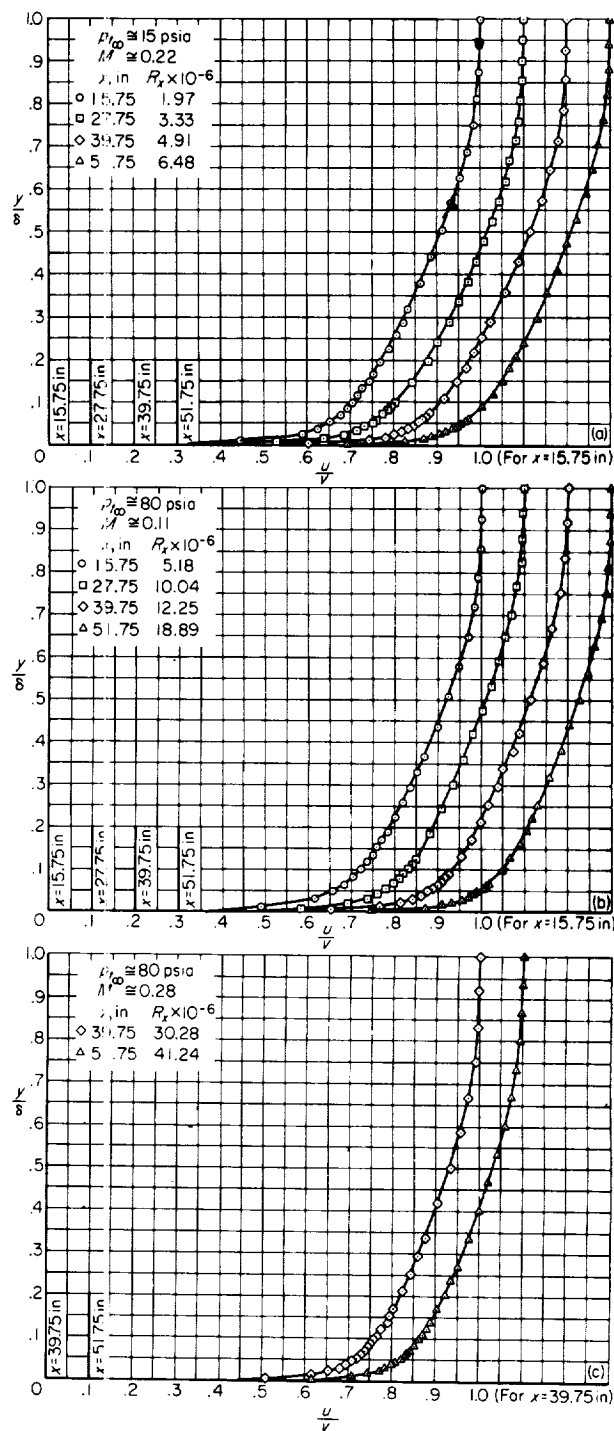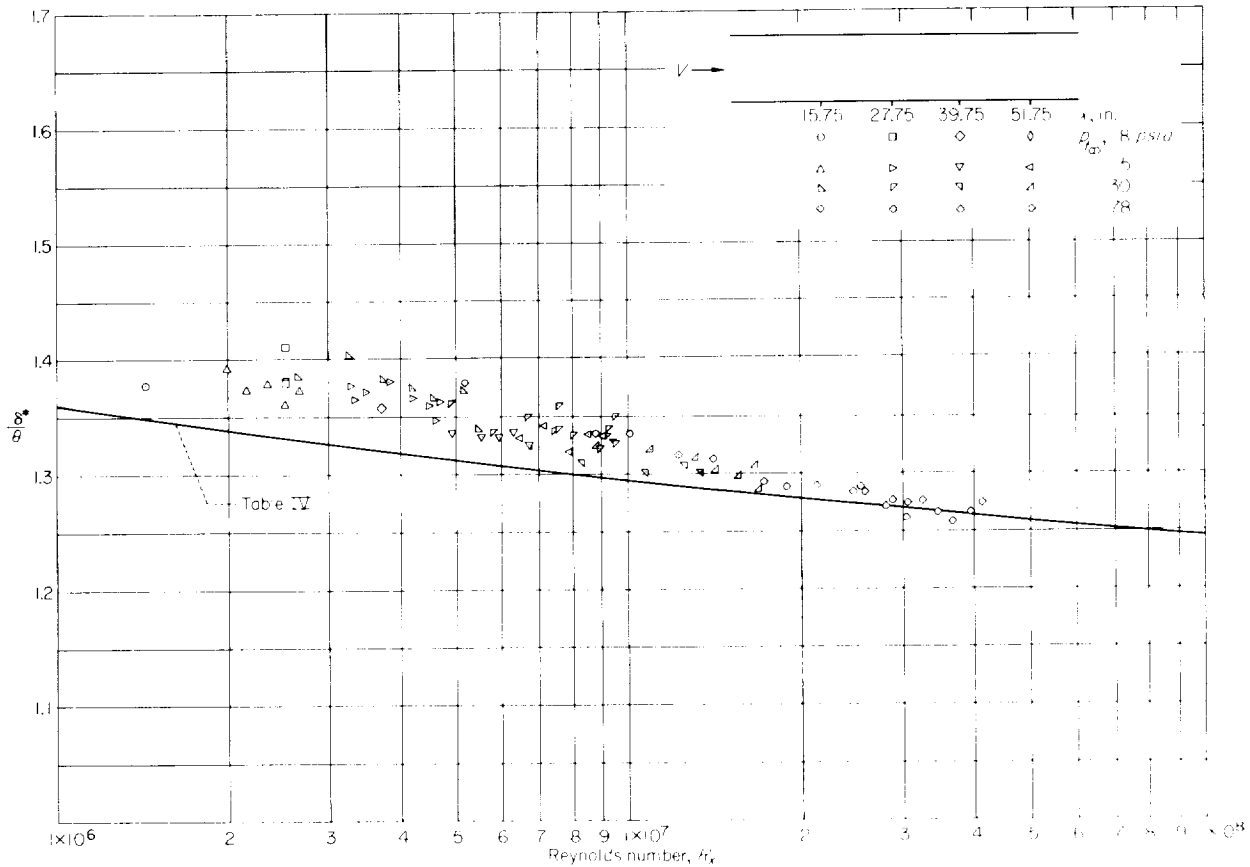

(a) $p_{t\infty} = 15$ psia, $M = 0.22$

(b) $p_{t\infty} = 80$ psia, $M = 0.11$

(c) $p_{t\infty} = 80$ psia, $M = 0.28$

FIGURE 10.—Boundary-layer velocity profiles.

FIGURE 11.- Variation of shape parameter with change in Reynolds number, R_x.

the shape parameter decreased as the Reynolds number increased. There appears to be large scatter in the data but this is not surprising since it is very difficult to obtain accurate values for either δ^* or θ. The line identified as table IV in this figure and in figures 12 and 13 will be discussed in a subsequent section.

The variation of the average skin-friction coefficient with change in Reynolds number is presented in figure 12. The average skin friction, C_F, was computed using the momentum thickness obtained from integration of the velocity profiles (presented in table III) measured at several stations along the wall of the channel. The Schoenherr line obtained from reference 11 will be discussed in a subsequent section.

There are presented in figure 13 the results of the measurement of the surface-shear stress. These results are tabulated in table II. The surface-shear stress was measured by the floating-element technique previously described.

COMPUTATION OF DRAG BY MOMENTUM DEFECT AND BY INTEGRATION OF LOCAL SKIN FRICTION

The friction drag of a surface can be computed by two methods. The first of these methods involves computation, by mechanical integration of the boundary-layer profile, of the loss of momentum in the boundary layer which is directly convertible to the drag loss (data of fig. 12). The second method consists of integration of the local surface shear along the surface which is also directly convertible to the drag loss (data of fig. 13). A difficulty is involved in the second method in that it is necessary to know the local skin friction right up to the origin of the turbulent boundary layer. To circumvent this problem in the present investigation the drag at a point 18 inches aft of the leading edge of the surface of the channel was assumed to be that obtained by the momentum defect method. The local skin friction was then integrated and added to the assumed value of drag which resulted in a total drag at a particular
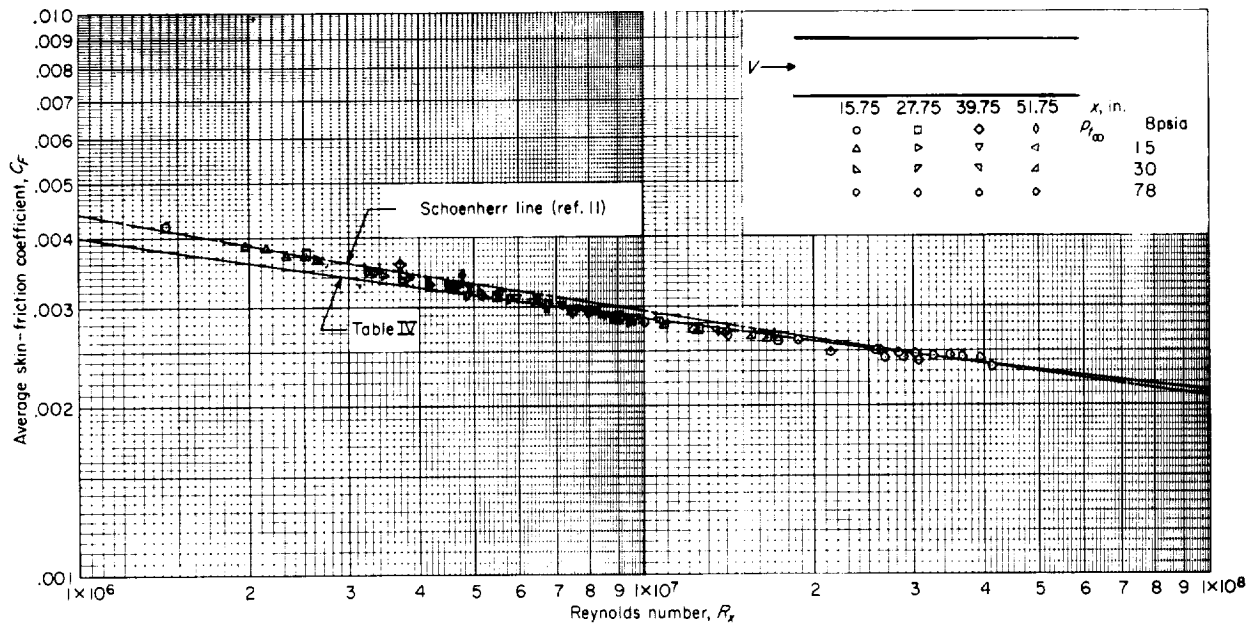
FIGURE 12.—Variation of average skin-friction coefficient with change in Reynolds number, R_x; boundary-layer velocity profile measurements
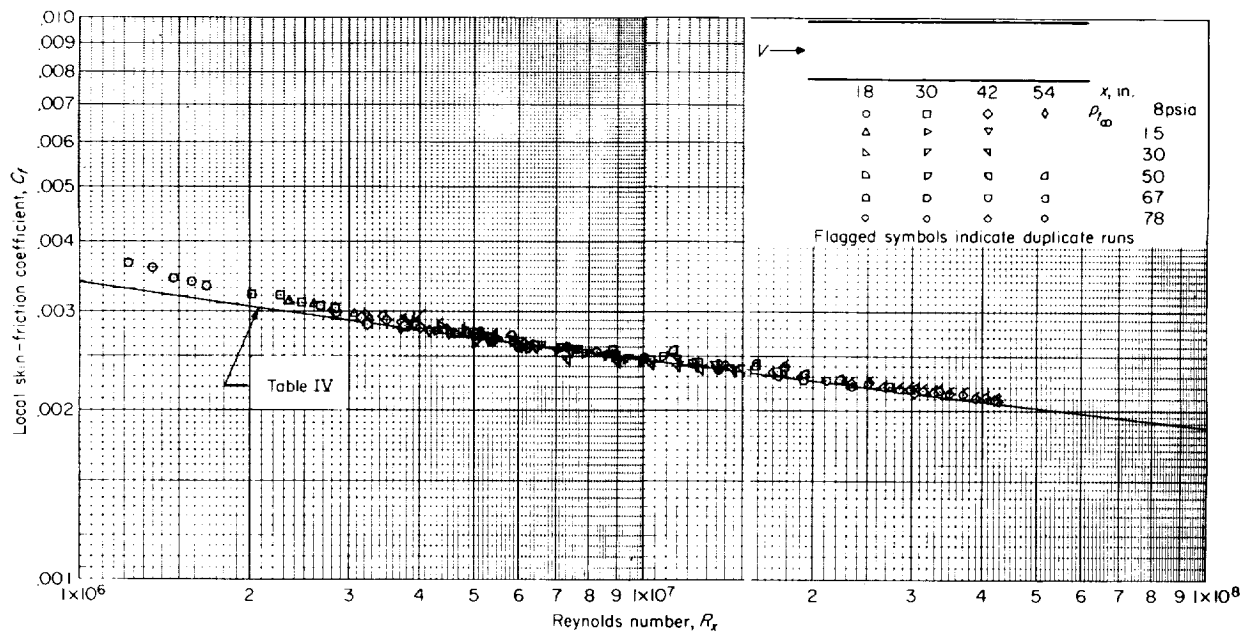
FIGURE 13.—Variation of local skin-friction coefficient with change in Reynolds number, R_x; floating-element technique.

longitudinal position on the channel wall. There are presented in figure 14 the results of these computations. The drag obtained by the momentum defect method is compared with that obtained by the integration of the local surface-shear stresses. Again it is pointed out that the drag at a point

18 inches aft of the leading edge is assumed to be the same for both methods. It is apparent that at the smaller values of Reynolds number there is a discrepancy between the drag obtained by the two methods. At a Reynolds number of about 6.5 million the drag obtained from the integrated

(a) $R_x \times 10^{-6} = 2.19$ to 6.56

(b) $R_x \times 10^{-6} = 5.95$ to 17.86

(c) $R_x \times 10^{-6} = 14.70$ to 44.10

FIGURE 14.—Comparison of drag computed by both the momentum defect and integrated surface-shear methods.

surface shear is about 4 percent higher than that obtained by the momentum defect, while at the highest Reynolds number of about 44 million the discrepancy between the two drags is reduced to almost zero.
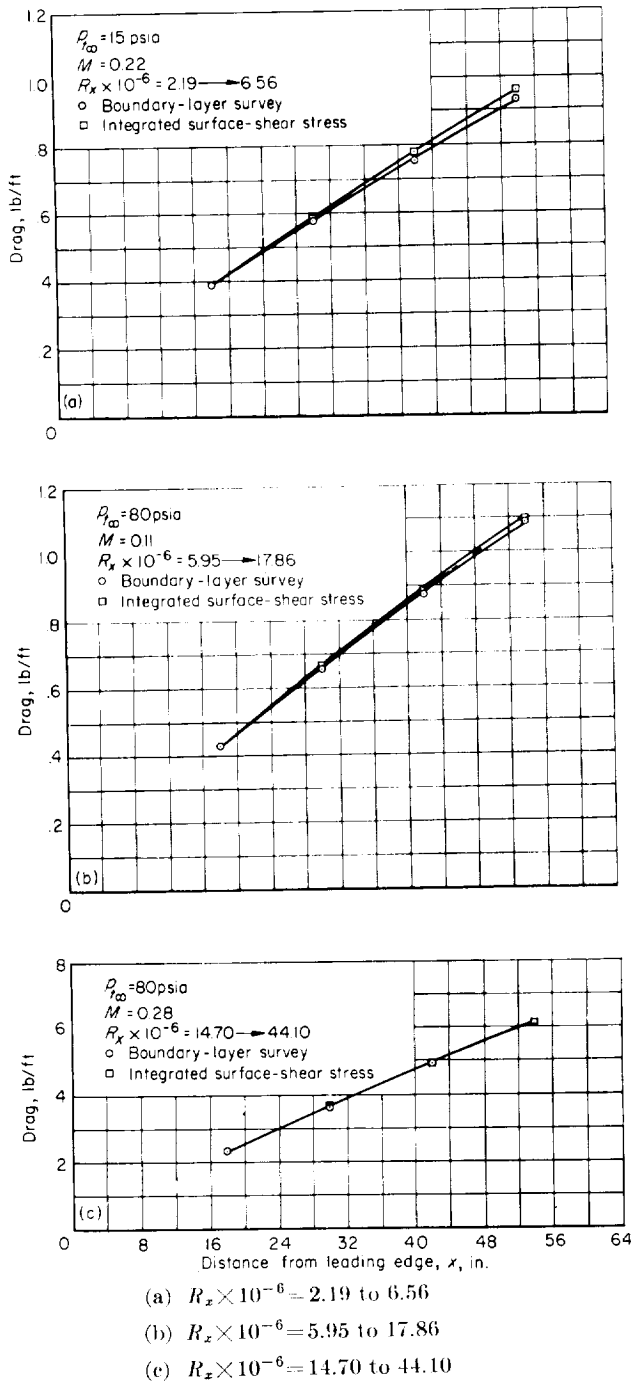
METHOD OF DATA ANALYSIS

The aforementioned data will be discussed further in conjunction with a method of boundary-layer analysis previously used by Coles and others and described in some detail in reference 12. It is not felt that a detailed reiteration of the method is necessary here. The use of this method facilitates the analysis of the data of the present investigation in a systematic manner.

The equations of reference 12 which are used in the present analysis are given below in the notation of this report.

$$C_f R_x = 2C_1 e^{-k\varphi(1)} e^{k\sqrt{2/C_f}} \left[1 - \left(\frac{2}{k} + \frac{C_2}{C_1}\right)\sqrt{\frac{C_f}{2}} + \frac{1}{k}\left(\frac{1}{k} + \frac{C_2}{C_1}\right)C_f \right]$$

$$C_F R_x = 2C_1 e^{-k\varphi(1)} e^{k\sqrt{2/C_f}} \left(1 - \frac{C_2}{C_1}\sqrt{\frac{C_f}{2}}\right)$$

$$\frac{\delta^*}{\theta} = \frac{1}{1 - \frac{C_2}{C_1}\sqrt{\frac{C_f}{2}}}$$

$$R_\theta = \frac{C_F R_x}{2}$$

The analysis depends on the evaluation of the parameters k, $\varphi(1)$, C_1, and C_2 which appear in the above equations.

The first step in the analysis is to express the velocity profiles in terms of the "law of the wall" $[u/u^* = f(yu^*/\nu)]$ and the "velocity defect law" $[(V-u)/u^* = f(yu^*/\delta^* V)]$. A typical profile in terms of the "wall law" is presented in figure 15(a) while the same profile in terms of the "velocity defect law" is presented in figure 15(b). As may be noted on these figures both curves have a linear region when plotted on a semilogarithmic basis. From a comparison of the slopes of the linear portions of these curves it appears that they both have the same value. This portion of the curves is known in the literature as the region of overlap of the two laws or the region of similarity of the boundary layer. The existence of this region of similarity makes it possible to analyze the turbulent boundary layer quite readily. With the velocity profiles in this form the parameters k and $\varphi(1)$ may be evaluated. The parameter k is the slope of the curves in the similarity region.

The parameter $\varphi(1)$ is the sum of the value of $\varphi(0)$ obtained from the wall law as shown in figure 15(a) and the value of $\varphi(1) - \varphi(0)$ obtained from the velocity defect law as shown in figure 15(b). The two parameters C_1 and C_2 are obtained from the velocity profile parameters as indicated by the definition given in the Notation section. The values of the four parameters k, $\varphi(1)$, C_1, and C_2 may then be inserted in the skin-friction equations given previously to calculate a frictional resistance law for a fully developed turbulent boundary layer which starts at some point with zero thickness and grows as a fully developed turbulent boundary layer.

The variation of the parameters k, $\varphi(0)$ and $\varphi(1) - \varphi(0)$ with Reynolds number, R_θ (based on the boundary-layer momentum thickness), is shown in figure 16, while the variation with R_θ of C_1 and C_2 is shown in figure 17. It is expected that these turbulent boundary-layer parameters will become independent of Reynolds number if they are determined from measurements at large enough Reynolds numbers on an aerodynamically smooth plate in flow having zero pressure gradient. This appears to be the case in the present experiments for Reynolds numbers, R_θ, greater than about 26 thousand or a Reynolds number, R_x, of about 21 million. The average value of the constants in the range of Reynolds number independence were used in conjunction with the skin-friction equations given previously to make calculations of a frictional resistance law. The values of the constants used in this calculation were:

$$\varphi(1) - \varphi(0) = 3.00$$
$$\varphi(0) = 7.15$$
$$k = 5.00$$
$$C_1 = 4.00$$
$$C_2 = 25.9$$

The results of this calculation are presented in table IV.

As a result of the scatter in the values of these parameters, which were obtained from the experimental data, and the limited Reynolds number range attained in this investigation, there is some doubt as to the absolute values of the parameters listed above. Hence, a new frictional resistance law is not being proposed although the results of the calculation have been tabulated and presented in this form to afford a basis of com-

(a) Wall law.

(b) Velocity defect law.
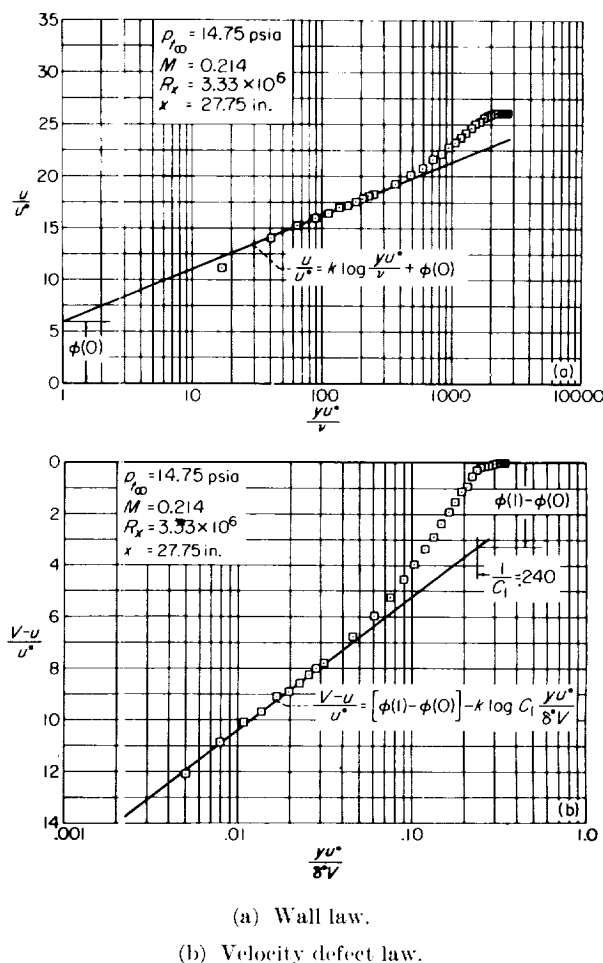
FIGURE 15.—Boundary-layer velocity profiles in terms of the "wall law" and the "velocity defect law."

parison between the measured data of the present investigation and those of previous investigations.

COMPARISON OF COMPUTED FRICTION LAW WITH MEASURED DATA

The results of the frictional resistance law calculation presented in table IV are also presented in figures 11, 12, and 13. As was previously stated, constants applicable only in the range of Reynolds number above about 21 million were used in this calculation.

Shape parameter.—As may be seen in figure 11, the computed values of the shape parameter, δ^*/θ presented in table IV represent those computed from the measured velocity profiles only at the highest Reynolds numbers. This is not difficult to understand when it is realized that the computed value of the shape parameter
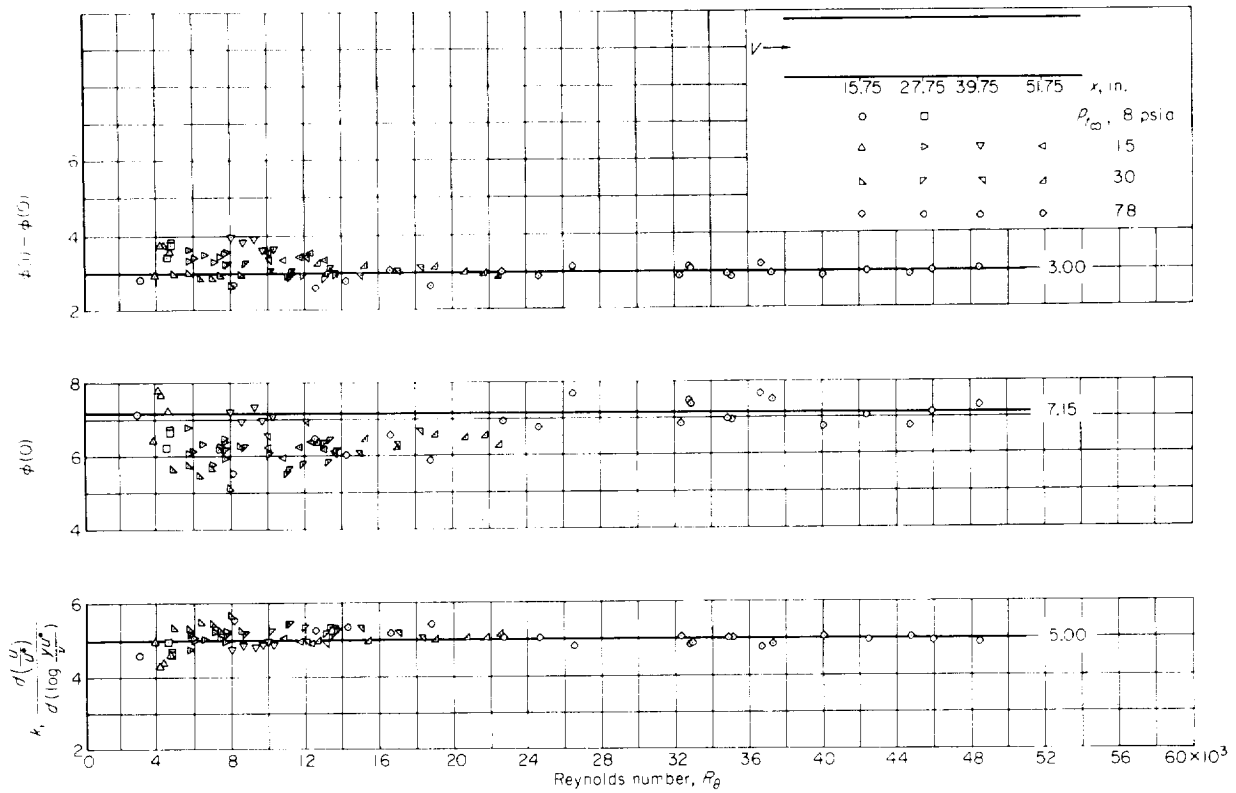
FIGURE 16.—Variation of K, $\varphi(0)$, and $\varphi(1) - \varphi(0)$ with change in Reynolds number, R_θ.
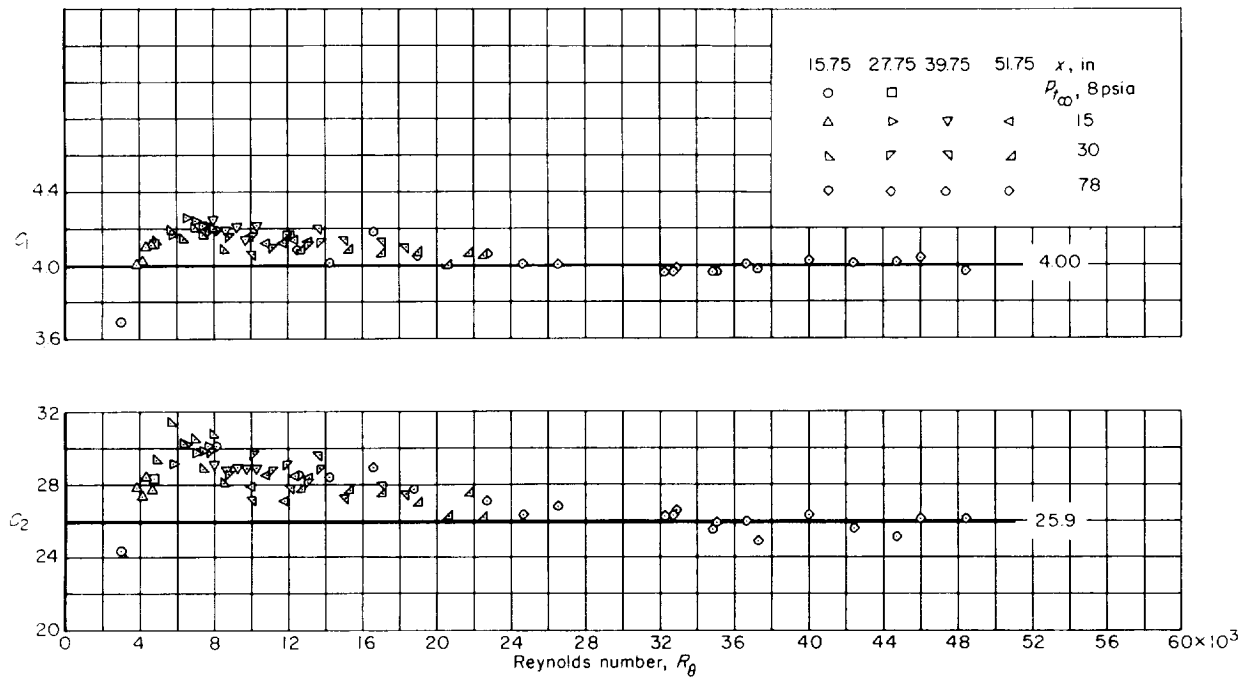
FIGURE 17.—Variation of C_1 and C_2 with change in Reynolds number, R_θ.

is dependent principally on C_1 and C_2, both of which change markedly below Reynolds numbers of about 21 million from the asymptotic value used in the computation (see fig. 17).

Average and local skin-friction coefficient.—It appears in figures 12 and 13 that the computed values of both the average skin-friction coefficient and the local skin-friction coefficient represent the measured values quite well for Reynolds numbers as low as about five or six million. The scatter in the data presented for both the average and local

skin-friction coefficients is represented generally by a change of skin friction of about ± 1 percent, and this s also about the variation of the measured
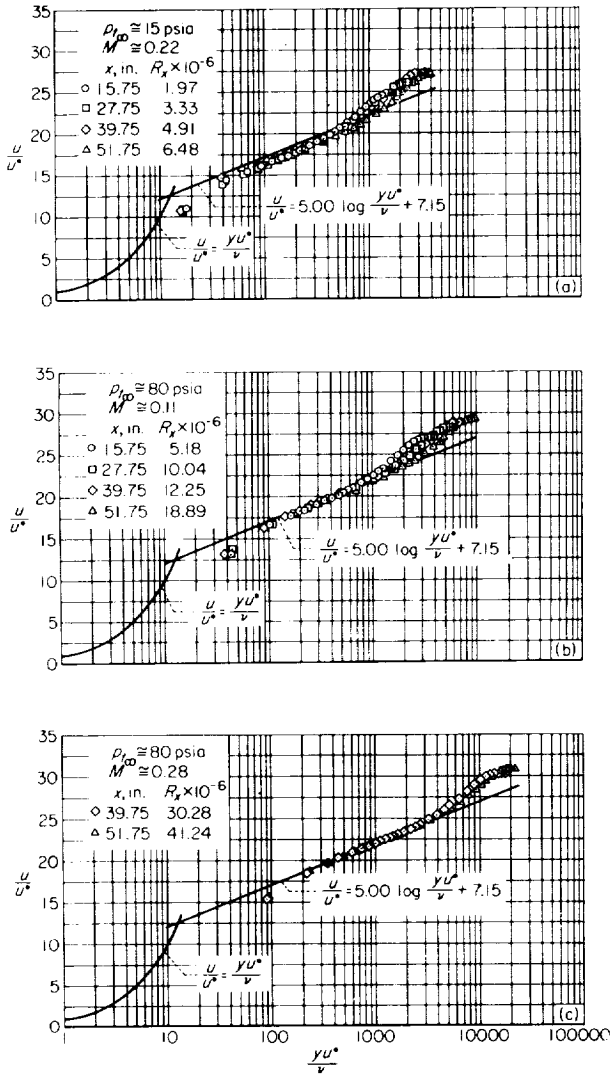
(a) $p_{t\infty} = 15$ psia, $M = 0.22$

(b) $p_{t\infty} = 80$ psia, $M = 0.11$

(c) $p_{t\infty} = 80$ psia, $M = 0.28$

FIGURE 18.—Boundary-layer velocity profiles in terms of the "wall law."

(a) $p_{t\infty} = 15$ psia, $M = 0.22$

(b) $p_{t\infty} = 80$ psia, $M = 0.11$

(c) $p_{t\infty} = 80$ psia, $M = 0.28$

FIGURE 19.—Boundary-layer velocity profiles in terms of the "velocity-defect law."

FIGURE 20.—Comparison of previous existing data with the measured data and with the curve computed using the constants derived from the present data.
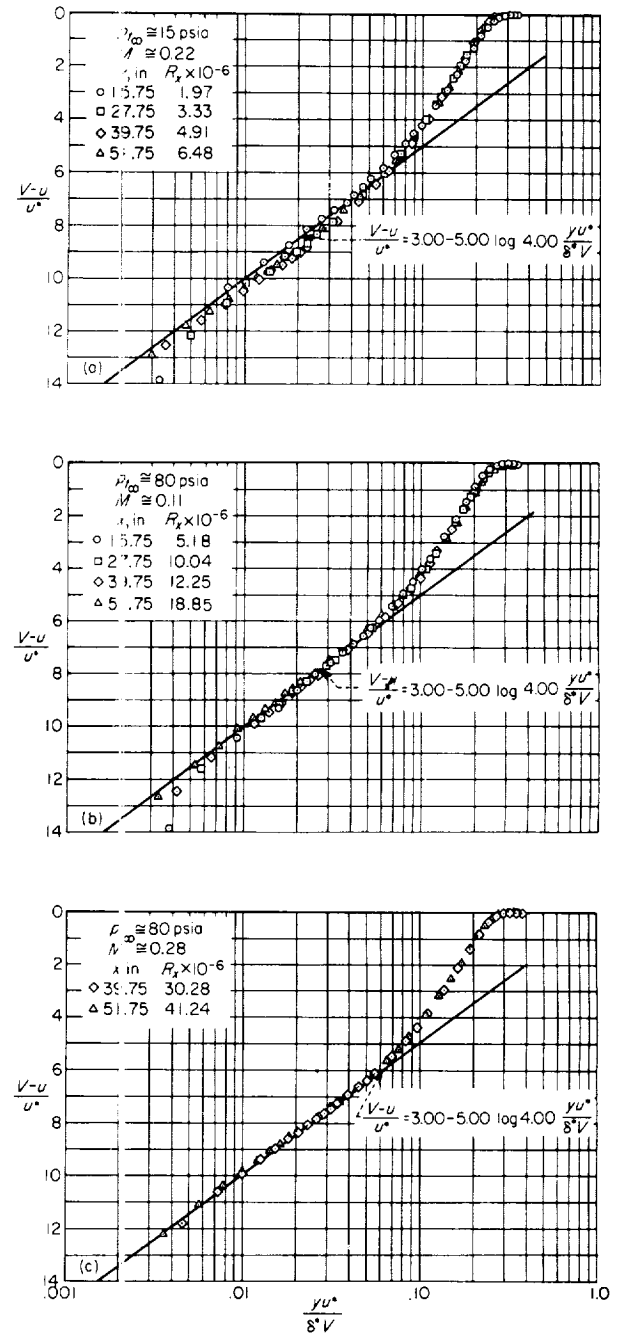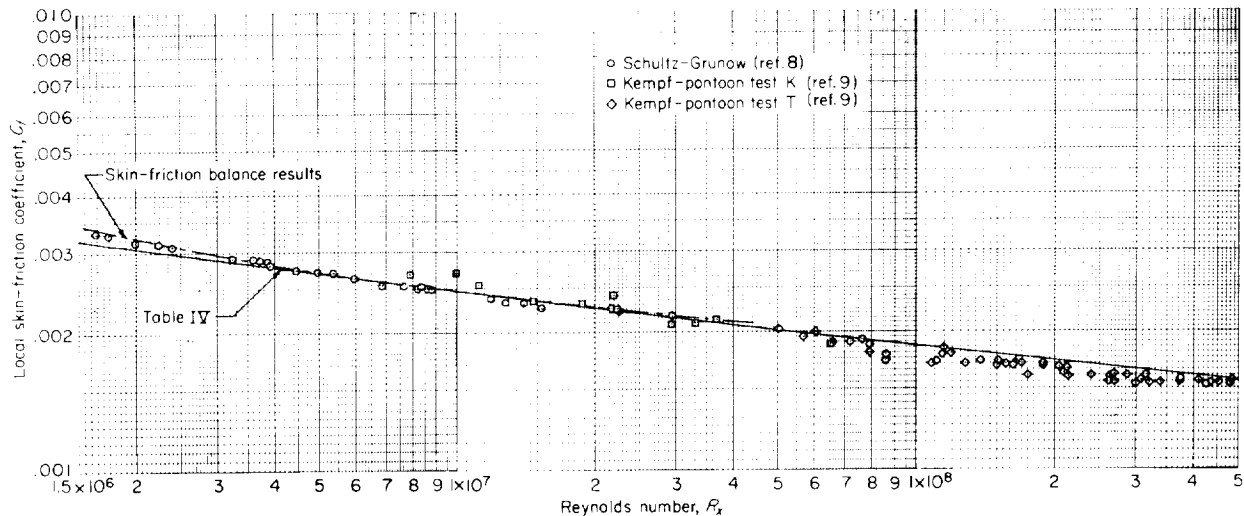
from the computed skin-friction coefficient at higher Reynolds numbers.

Law of the wall and velocity-defect law.—In figures 18 and 19 it is shown that the wall law and velocity-defect law derived using the value of the constants in the range of Reynolds number independence do not represent the measured data except at the higher values of Reynolds number. Here again this is easily understood after inspection of the variation with Reynolds number, shown in figure 16, of the parameters used in both laws.

COMPARISON OF MEASURED DATA AND COMPUTED FRICTION LAW WITH MEASURED DATA OF OTHER INVESTIGATIONS

Local skin-friction coefficients.—There are presented in figure 20 the local skin-friction coefficients measured by Schultz-Grunow (ref. 8) in an air channel and by Kempf (ref. 9) on a pontoon in water. In the region of Reynolds number where the two sets of data overlap, Kempf's data appear to be somewhat higher than those of Schultz-Grunow. In this region of overlap, Schultz-Grunow's data agree quite well with the skin-friction balance results. Comparison of the measured local skin-friction-coefficient data of the present investigation with those of both Schultz-Grunow and Kempf indicates remarkable agreement in the Reynolds number range of the investigation when it is considered that the data came from three grossly different pieces of equipment. Here, as in figure 13, there is a tendency for the measured data to be higher than the com-

puted friction law (table IV) for Reynolds numbers smaller than about 4 or 5 million. However, the computed friction law does match the measured data quite well for a range of Reynolds numbers from 4 or 5 million to about 60 million. For Reynolds numbers above 60 million Kempf's data appear to fall below the line representing the computed law.

Average skin-friction coefficient.—A comparison of the measured average skin-friction coefficients of the present investigation with the Schoenherr line (ref. 11) is presented in figure 12. The Schoenherr line gives larger values of skin friction than were measured in the present investigation for Reynolds numbers from 3 to 30 million, but became equal to the measured values at Reynolds number from 1 to 3 million and from 30 to 45 million. The measured data are best represented by the Schoenherr line in the range of Reynolds numbers from 1 to 3 million and by the computed law (table IV) in the range of Reynolds numbers from 5 to 45 million.

Figure 21 is a reproduction of a figure presented in reference 11 with the exception that the computed friction law of the present investigation is also presented for comparison. The friction law as computed from the data of the present investigation gives values of skin-friction coefficient as much as 8 percent lower than the Schoenherr line at a Reynolds number of 1 million and as much as 6 percent higher at a Reynolds number of 1×10^9. Similar to previous comparisons be-
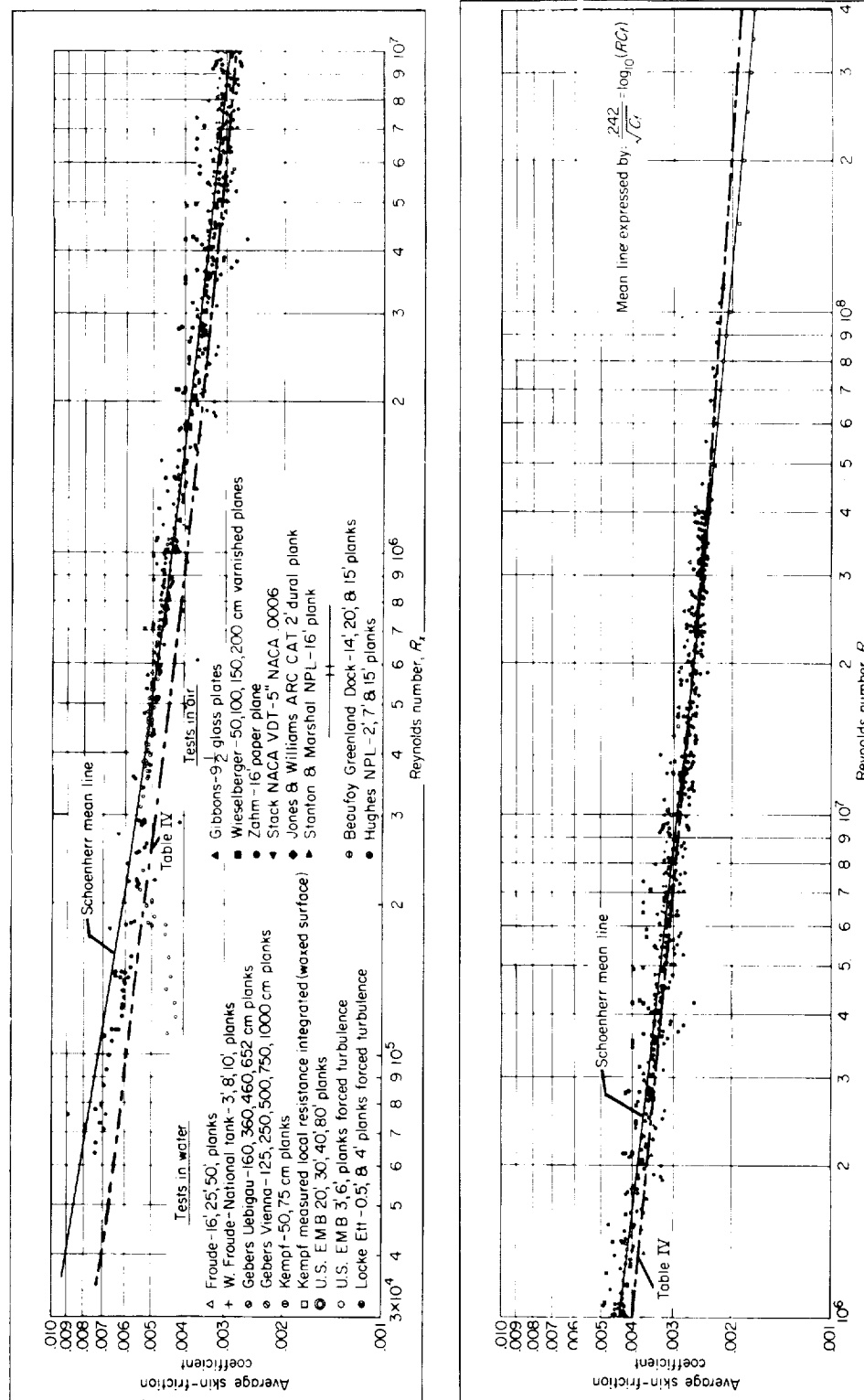
FIGURE 21.—Comparison of previous existing data with computed friction law (table IV).
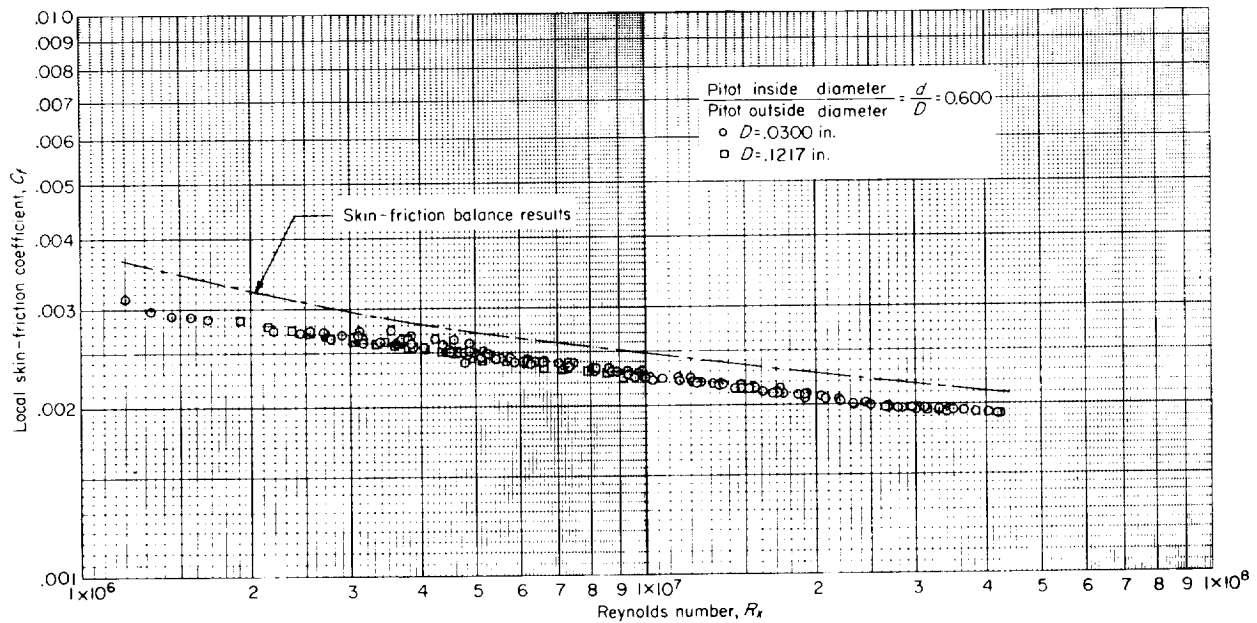
FIGURE 22. Variation of local skin-friction coefficient with change in Reynolds number, R_x; Preston tube technique.

tween the computed curve and the measured data, the measured data are somewhat higher in the low Reynolds number range. In the range of Reynolds number from 5 million to 100 million the computed law seems to represent the data quite well. Beyond a Reynolds number of 100 million there is only one set of data available to compare with the computed values and they lie below the computed line for all higher values of Reynolds number.

A SIMPLE METHOD FOR DETERMINING LOCAL SURFACE-SHEAR STRESS IN A TURBULENT BOUNDARY LAYER

There are presented in figure 22 the results of measurements of local skin-friction coefficient using a calibrated total-head tube as proposed by J. H. Preston in 1953 and previously described in the section on experimental methods. On the same figure is presented a line representing the faired value of the data measured with the floating-element device as presented previously in figure 13. In general, the Preston tube device indicates a smaller skin friction than the floating-element device. However, the results of both methods can be made to agree quite well if the calibration presented by Preston in reference 5 is modified slightly.

From the work of Preston it has been shown that the calibration of the tubes is valid only if the value of the expression $\log_{10} \frac{(p_t - p)d^2}{4\rho\nu^2}$ is

greater than about 5.0 but less than about 7.5. These limiting values also seem to be the limiting values obtained in the present investigation. When the value of the expression $\log_{10} \frac{(p_t - p)d^2}{4\rho\nu^2}$ falls outside of these limits the measured skin friction immediately varies away from the general trend of similar data measured at the same Reynolds number when the value of the logarithmic expression falls within the prescribed values.

It appears that the Preston tube device can be quite useful in measuring the local surface-shear stress in a turbulent boundary layer where the longitudinal static-pressure gradient is zero. Not only does it appear to be accurate but it is extremely simple and inexpensive to construct. Also, the indicating equipment is simple and readily available to most investigators.

For Reynolds numbers greater than 2.5 million the revised calibration suggested by the measured surface-shear stress data obtained on the floating-element device is

$$\log_{10} \frac{\tau_w d^2}{4\rho\nu^2} = -1.366 + 0.877 \log_{10} \frac{(p_t - p)d^2}{4\rho\nu^2}$$

as compared with Preston's calibration of reference 5,

$$\log_{10} \frac{\tau_w d^2}{4\rho\nu^2} = -1.396 + 0.875 \log_{10} \frac{(p_t - p)d^2}{4\rho\nu^2}$$

For Reynolds numbers lower than 2.5 million use

of the revised calibration results in values of surface shear which are lower than the measured data.

CONCLUDING REMARKS

The measured local skin-friction coefficients obtained from the floating-element skin-friction balance agree well with the long accepted experimental data of Schultz-Grunow and Kempf in the range of Reynolds numbers from about 1 million to about 45 million.

The average skin-friction coefficients deduced from the measured velocity profiles are generally below the Schoenherr line except at the lowest values of Reynolds number. As the Reynolds number approached 45 million, the highest value attained in the present investigation, the measured average skin friction became equal to the value predicted by Schoenherr. However, the rate of change of the measured average skin-friction coefficient with increasing Reynolds number is smaller than that predicted by Schoenherr.

The frictional drag experienced by a flat-plate surface has been computed by both the momentum-defect method and the integration of the local surface shear. At values of Reynolds number from 14 million to 45 million the results of both methods are in good agreement but show a discrepancy of as much as 4 percent in the range of Reynolds numbers from 2 to 6 million.

In the light of the data of the present investigation a new frictional resistance law for a smooth plate having zero pressure gradient may be written. However, there is some doubt as to the absolute values of the experimentally determined parameters which must be used in conjunction with the skin-friction equations to write a law. These parameters appear to approach asymptotically a constant value, as was anticipated. As a result of the scatter in the values of the parameters obtained from the experimental data and the limited Reynolds number range attained in the investigation, there seems to be some doubt as to the validity of a law written on the basis of these parameters.

The local skin friction determined from measurements utilizing a calibrated pitot tube mounted on the surface as proposed by J. H. Preston had a lower value than that measured by the floating-element skin-friction balance. However, a small adjustment of Preston's calibration of the pitot tube brought the two results into good agreement.

The Preston pitot tube appears to be an inexpensive and accurate device for making local surface-shear-stress measurements.

AMES RESEARCH CENTER
   NATIONAL AERONAUTICS AND SPACE ADMINISTRATION
   MOFFETT FIELD, CALIF., Dec. 9, 1957

REFERENCES

1. Telfer, E. V.: Further Ship Resistance Similarity. Trans. Inst. Naval Architects, vol. 93, no. 4, Oct. 1951, pp. 205–226.
2. Telfer, E. V.: Frictional Resistance and Ship Resistance Similarity. Trans. Inst. Naval Architects, vol. 92, no. 1, Jan. 1951, pp. 1–27.
3. Hughes, G.: Frictional Resistance of Smooth Plane Surfaces in Turbulent Flow. New Data and a Survey of Existing Data. Trans. Inst. Naval Architects, vol. 94, no. 4, Oct. 1952, pp. 287–322.
4. Todd, Dr. F. H.: Skin Friction Resistance and the Effects of Surface Roughness. Paper presented at summer meeting of The Society of Naval Architects and Marine Engineers in Washington, D. C., Sept. 6–7, 1951. (Also David W. Taylor Model Basin Rep. 729, 1950)
5. Preston, J. H.: The Determination of Turbulent Skin Friction by Means of Pitot Tubes. British ARC Fluid Motion Sub-Com. No. 15,758, March 31, 1953.
6. Fage, A., and Sargent, R. F.: An Air-Injection Method of Fixing Transition from Laminar to Turbulent Flow in a Boundary Layer. ARC R. & M. No. 2106, June 1944. (Issued as: ARC, Aerodynamics Sub-Com. 7800, June 12, 1944)
7. Dhawan, Statish: Direct Measurements of Skin Friction. NACA Rep. 1121, 1953. (Supersedes NACA TN 2567)
8. Schulz-Grunow, F.: New Frictional Resistance Law for Smooth Plates. NACA TM 986, 1941. (Also Luftfahrtforschung, vol. 17, no. 8, Aug. 20, 1940, pp. 239–246)
9. Kempf, von Gunther: Wietere Reibungsergebnisse an ebenen glatten und rauhen Flächen. Hydrodynamische Probleme des Schiffsantriebs, vol. 1, 1932, pp. 74–82.
10. Rubesin, Morris W., Maydew, Randall C., and Varga, Steven A.: An Analytical and Experimental Investigation of the Skin Friction of the Turbulent Boundary Layer on a Flat Plate at Supersonic Speeds. NACA TN 2305, 1951.
11. Locke, F. W. S., Jr.: Recommended Definition of Turbulent Friction in Incompressible Fluid. Navy Dept., Bureau of Aeronautics, Research Div., DR Rep. 1415, June 1952.
12. Coles, Donald: Measurements in the Boundary Layer on a Smooth Flat Plate in Supersonic Flow. I. The Problem of the Turbulent Boundary Layer. Rep. 20–69, C.I.T. Jet Propulsion Lab., Pasadena, June 1, 1953.

TABLE 1.—MEASURED BOUNDARY-LAYER VELOCITY PROFILES

(a) x = 15.75 inches

$R_x \times 10^{-6}$		1.43		1.97		2.16		2.33		2.51		2.64		2.65		3.21
$p_{(\infty)}$ (psia)		7.94		15.17		14.81		14.83		14.84		15.86		25.41		25.65
$T(°F)$		76		71		72		73		78		81		69		73
M		0.308		0.215		0.211		0.204		0.208		0.307		0.152		0.187
y, inch	u/V	y, inch	u/V	y, inch	u/V	y, inch	u/V	y, inch	u/V	y, inch	u/V	y, inch	u/V	y, inch	u/V
0.0035	0.426	0.0035	0.446	0.0035	0.474	0.0035	0.478	0.0035	0.485	0.0035	0.488	0.0035	0.459	0.0035	0.498
.0085	.589	.0085	.586	.0085	.598	.0085	.601	.0085	.589	.0085	.606	.0085	.587	.0085	.591
.0135	.631	.0135	.625	.0135	.638	.0135	.636	.0135	.636	.0135	.638	.0135	.625	.0135	.634
.0175	.646	.0185	.651	.0185	.653	.0185	.656	.0185	.656	.0185	.661	.0185	.653	.0185	.656
.0235	.671	.0235	.676	.0235	.671	.0235	.671	.0235	.676	.0235	.671	.0235	.674	.0235	.680
.0285	.689	.0285	.693	.0285	.691	.0285	.692	.0285	.695	.0285	.685	.0285	.692	.0285	.695
.0335	.701	.0335	.701	.0335	.705	.0335	.705	.0335	.709	.0335	.711	.0335	.707	.0335	.713
.0385	.713	.0385	.715	.0385	.717	.0385	.718	.0385	.722	.0385	.724	.0385	.720	.0385	.724
.0435	.726	.0435	.727	.0435	.726	.0435	.731	.0435	.734	.0435	.736	.0435	.733	.0435	.736
.0485	.736	.0485	.740	.0485	.739	.0485	.740	.0485	.743	.0485	.747	.0485	.743	.0485	.748
.0535	.746	.0535	.752	.0535	.750	.0535	.753	.0535	.754	.0535	.756	.0535	.754	.0535	.759
.0635	.765	.0635	.768	.0635	.770	.0635	.772	.0635	.774	.0635	.773	.0635	.775	.0635	.779
.0735	.781	.0735	.787	.0735	.788	.0735	.789	.0735	.791	.0735	.789	.0735	.792	.0735	.799
.0835	.796	.0835	.804	.0835	.803	.0835	.807	.0835	.809	.0835	.795	.0835	.808	.0835	.815
.0935	.809	.0935	.820	.0935	.820	.0935	.824	.0935	.825	.0935	.814	.0935	.827	.0935	.832
.1035	.824	.1035	.832	.1035	.837	.1035	.839	.1035	.841	.1035	.824	.1035	.842	.1035	.848
.1235	.851	.1235	.862	.1235	.864	.1235	.868	.1235	.872	.1235	.844	.1235	.871	.1235	.877
.1435	.875	.1435	.886	.1435	.890	.1435	.896	.1435	.896	.1435	.871	.1435	.899	.1435	.905
.1635	.900	.1635	.911	.1635	.919	.1635	.919	.1635	.922	.1635	.898	.1635	.923	.1635	.928
.1835	.917	.1835	.932	.1835	.936	.1835	.942	.1835	.944	.1635	.926	.1835	.944	.1835	.949
.2035	.936	.2035	.951	.2035	.955	.2035	.960	.2035	.963	.1835	.947	.2035	.963	.2035	.968
.2235	.952	.2235	.966	.2235	.970	.2235	.976	.2235	.974	.2035	.967	.2235	.981	.2235	.982
.2435	.968	.2435	.981	.2435	.983	.2435	.988	.2435	.989	.2235	.980	.2435	.989	.2435	.991
.2635	.979	.2635	.990	.2635	.992	.2635	.996	.2635	.997	.2135	.940	.2635	.995	.2635	.996
.2835	.987	.2835	.996	.2835	.996	.2835	.996	.2835	1.000	.2635	.957	.2835	1.000	.2835	.998
.3035	.992	.3035	.999	.3035	.999	.3035	1.000			.2835	1.000				
.3235	.994	.3235	1.000							.3035	1.000				
.3435	.996														
.3635	.997														
.3865	.997														

TABLE I.—MEASURED BOUNDARY-LAYER VELOCITY PROFILES—Continued

(a) x=15.75 inches—Concluded

$r_x \times 10^{-6}$	3.72	4.16	4.56	5.13	5.48	5.18	8.82
p_∞ (psia)	28.94	29.25	29.57	30.73	30.52	78.45	78.83
T (°F)	78	81	82	84	78	69	80
M	0.216	0.243	0.265	0.289	0.308	0.107	0.188

Group $r_x \times 10^{-6} = 3.72$:

y, inch	u/U
0.0035	0.475
.0085	.598
.0135	.641
.0185	.667
.0235	.689
.0285	.706
.0335	.721
.0385	.734
.0435	.745
.0485	.756
.0535	.767
.0635	.787
.0735	.845
.0835	.823
.0935	.839
.1035	.854
.1235	.884
.1435	.911
.1635	.936
.1835	.956
.2035	.973
.2235	.986
.2435	.994
.2635	.998
.2835	.999

Group $r_x \times 10^{-6} = 4.16$:

y, inch	u/U
0.0035	0.480
.0085	.605
.0135	.648
.0185	.674
.0235	.696
.0285	.712
.0335	.726
.0385	.739
.0435	.750
.0485	.761
.0535	.771
.0635	.792
.0735	.810
.0835	.827
.0935	.844
.1035	.858
.1235	.880
.1435	.916
.1635	.940
.1835	.960
.1935	.968
.2035	.976
.2235	.989
.2435	.994
.2635	.998
.2835	.999

Group $r_x \times 10^{-6} = 4.56$:

y, inch	u/U
0.0035	0.520
.0085	.619
.0135	.656
.0185	.682
.0235	.702
.0285	.719
.0335	.731
.0385	.744
.0435	.755
.0485	.766
.0535	.777
.0635	.795
.0735	.814
.0835	.832
.0935	.849
.1035	.864
.1235	.898
.1435	.919
.1635	.943
.1835	.963
.2035	.978
.2235	.990
.2435	.996
.2635	.999
.2835	.999

Group $r_x \times 10^{-6} = 5.13$:

y, inch	u/U
0.0035	0.484
.0085	.612
.0135	.656
.0185	.682
.0235	.702
.0285	.722
.0335	.738
.0385	.750
.0435	.759
.0485	.770
.0535	.780
.0635	.801
.0735	.820
.0835	.836
.0935	.853
.1035	.868
.1235	.884
.1435	.921
.1635	.947
.1835	.966
.2035	.981
.2235	.991
.2435	.997
.2635	1.000
.2835	1.000

Group $r_x \times 10^{-6} = 5.48$:

y, inch	u/U
0.0035	0.524
.0085	.627
.0135	.645
.0185	.690
.0235	.709
.0285	.726
.0335	.739
.0385	.752
.0435	.764
.0485	.775
.0585	.784
.0635	.794
.0685	.814
.0735	.824
.0835	.840
.0935	.855
.1035	.872
.1235	.901
.1435	.925
.1635	.949
.1835	.969
.2035	.982
.2235	.993
.2435	.998
.2635	1.000
.2835	1.000

Group $r_x \times 10^{-6} = 5.18$:

y, inch	u/U
0.0035	0.488
.0085	.615
.0135	.656
.0185	.682
.0235	.704
.0285	.721
.0335	.735
.0385	.747
.0435	.758
.0485	.770
.0535	.780
.0635	.800
.0735	.817
.0835	.834
.0935	.851
.1035	.856
.1235	.847
.1435	.921
.1635	.945
.1835	.967
.2035	.982
.2235	.992
.2435	.997
.2635	.999
.2835	1.000
.3035	1.000
.3235	1.000

Group $r_x \times 10^{-6} = 8.82$:

y, inch	u/U
0.0035	0.541
.0085	.646
.0135	.684
.0185	.710
.0235	.730
.0285	.744
.0335	.758
.0385	.771
.0435	.782
.0485	.791
.0535	.803
.0635	.819
.0735	.857
.0835	.853
.0935	.870
.1035	.885
.1235	.904
.1435	.936
.1635	.959
.1835	.957
.2035	.986
.2235	.996
.2435	.999
.2635	1.000

TABLE I.—MEASURED BOUNDARY-LAYER VELOCITY PROFILES—Continued

(b) $x=27.75$ inches

$R_x \times 10^{-6}$	2.52		3.33		3.83		4.17		4.50		4.70		4.90		5.82	
$p_{t\infty}$ (psia)	1.77		14.75		15.01		15.07		15.01		14.91		29.51		29.45	
T (°F)	68		76		74		78		75		83		65		76	
M	0.309		0.211		0.242		0.266		0.288		0.310		0.152		0.186	
y, inch	u/U	y, inch	u/U	y, inch	u/U	y, inch	u/U	y, inch	u/U	y, inch	u/U	y, inch	u/U	y, inch	u/U
0.0035	0.391	0.0035	0.428	0.0035	0.433	0.0035	0.438	0.0035	0.446	0.0035	0.463	0.0035	0.451	0.0035	0.461
.0085	.533	.0085	.537	.0085	.554	.0095	.558	.0085	.560	.0085	.555	.0085	.564	.0085	.571
.0135	.580	.0135	.584	.0135	.588	.0135	.599	.0135	.601	.0135	.602	.0135	.601	.0135	.611
.0185	.599	.0185	.613	.0185	.615	.0185	.617	.0185	.624	.0185	.627	.0185	.629	.0185	.635
.0235	.617	.0235	.630	.0235	.636	.0235	.637	.0235	.645	.0235	.643	.0235	.647	.0235	.653
.0285	.631	.0285	.652	.0285	.654	.0285	.653	.0285	.658	.0285	.661	.0285	.662	.0285	.668
.0335	.645	.0335	.659	.0335	.666	.0335	.667	.0335	.672	.0335	.675	.0335	.679	.0335	.683
.0385	.657	.0385	.672	.0385	.675	.0385	.680	.0385	.684	.0385	.688	.0385	.680	.0385	.693
.0435	.666	.0435	.685	.0435	.686	.0435	.691	.0435	.693	.0435	.697	.0435	.699	.0435	.705
.0485	.676	.0485	.694	.0485	.696	.0485	.699	.0485	.703	.0485	.704	.0485	.709	.0485	.714
.0535	.687	.0535	.702	.0535	.705	.0535	.711	.0535	.713	.0535	.714	.0535	.719	.0535	.723
.0785	.723	.0785	.741	.0785	.711	.0785	.744	.0785	.750	.0785	.751	.0785	.755	.0785	.761
.1035	.753	.1035	.771	.1035	.773	.1035	.776	.1035	.780	.1035	.782	.1035	.787	.1035	.792
.1285	.781	.1285	.799	.1285	.799	.1285	.802	.1285	.807	.1285	.811	.1285	.814	.1285	.817
.1535	.805	.1535	.826	.1535	.826	.1535	.829	.1535	.832	.1535	.835	.1535	.839	.1535	.843
.1785	.828	.1785	.849	.1785	.850	.1785	.854	.1785	.856	.1785	.859	.1785	.862	.1785	.866
.2035	.851	.2035	.871	.2035	.871	.2035	.875	.2035	.880	.2035	.880	.2035	.884	.2035	.889
.2285	.872	.2285	.890	.2285	.891	.2285	.895	.2285	.900	.2285	.901	.2285	.905	.2285	.909
.2535	.894	.2535	.909	.2535	.911	.2535	.915	.2535	.918	.2535	.920	.2535	.923	.2535	.927
.2785	.909	.2785	.927	.2785	.929	.2785	.934	.2785	.935	.2785	.938	.2785	.940	.2785	.943
.3035	.926	.3035	.942	.3025	.946	.3035	.949	.3035	.952	.3035	.954	.3035	.956	.3035	.960
.3285	.942	.3285	.957	.3285	.960	.3285	.964	.3285	.967	.3285	.979	.3285	.970	.3285	.973
.3535	.956	.3535	.965	.3535	.971	.3535	.974	.3535	.977	.3535	.979	.3535	.982	.3535	.983
.3785	.968	.3785	.980	.3785	.982	.3785	.984	.3785	.986	.3785	.987	.3785	.989	.3785	.991
.4035	.977	.4035	.989	.4035	.990	.4035	.991	.4035	.992	.4035	.992	.4035	.994	.4035	.995
.4285	.986	.4285	.993	.4285	.995	.4285	.995	.4285	.995	.4285	.995	.4285	.997	.4285	.998
.4535	.991	.4535	.996	.4535	.997	.4535	.997	.4535	.997	.4535	.997	.4485	.998	.4535	.999
.4785	.994	.4785	.997	.4785	.998	.4785	.998	.4785	.998	.4785	.998	.4785	.999	.4785	.999
.5035	.996	.5035	.998	.5035	.999	.5035	.998	.5035	.998	.5035	.998	.5035	.999		
.5285	.997	.5285	.999	.5285	.999			.5285	.998	.5285	.998				
.5535	.997	.5535	.999					.5535	.998	.5535	.998				
.5785	.998	.5785	.999							.6035	.998				
.6035	.998														
.6285	.998														
.6535	.998														

TABLE I.—MEASURED BOUNDARY-LAYER VELOCITY PROFILES—Continued

(b) x=27.75 inches—Concluded

$R_x \times 10^{-6}$	6.74	7.58	8.27	9.00	9.60	10.04	14.08
$p_{t\infty}$ (psia)	29.46	29.10	29.62	30.32	30.63	85.28	84.93
T' (°F)	74	66	73	78	85	66	67
M	0.217	0.243	0.266	0.288	0.310	0.108	0.152

y, inch	u/V	y, inch	u/V	y, inch	u/V	y, inch	u/V	y, inch	u/V	y, inch	u/V	y, inch	u/V
0.0035	0.469	0.0035	0.473	0.0035	0.483	0.0035	0.479	0.0035	0.490	0.0035	0.482	0.0035	0.492
.0085	.578	.0085	.579	.0085	.587	.0085	.595	.0085	.596	.0085	.591	.0085	.603
.0135	.616	.0135	.619	.0135	.625	.0135	.629	.0135	.635	.0135	.636	.0135	.649
.0185	.644	.0185	.646	.0185	.653	.0185	.655	.0185	.661	.0185	.659	.0185	.673
.0235	.662	.0235	.666	.0235	.672	.0235	.676	.0235	.681	.0235	.678	.0235	.693
.0285	.678	.0285	.682	.0285	.687	.0285	.691	.0285	.696	.0285	.695	.0285	.709
.0335	.691	.0335	.696	.0335	.700	.0335	.703	.0335	.708	.0335	.708	.0335	.722
.0385	.703	.0385	.709	.0385	.712	.0385	.716	.0385	.719	.0385	.719	.0385	.733
.0435	.713	.0435	.717	.0435	.722	.0435	.727	.0435	.729	.0435	.729	.0435	.743
.0485	.722	.0485	.726	.0485	.730	.0485	.736	.0485	.738	.0485	.737	.0485	.751
.0535	.731	.0535	.734	.0535	.740	.0535	.744	.0535	.746	.0535	.747	.0535	.759
.0785	.767	.0785	.771	.0785	.774	.0785	.778	.0785	.781	.0785	.780	.0785	.792
.1035	.797	.1035	.799	.1035	.804	.1035	.807	.1035	.810	.1035	.809	.1035	.820
.1285	.824	.1285	.828	.1285	.830	.1285	.833	.1285	.836	.1285	.834	.1285	.847
.1535	.849	.1535	.852	.1535	.854	.1535	.858	.1535	.860	.1535	.859	.1535	.870
.1785	.870	.1785	.873	.1785	.878	.1785	.879	.1785	.882	.1785	.880	.1785	.891
.2035		.2035		.2035		.2035		.2035	.904	.2035	.901	.2035	.910
.2285	.913	.2285	.917	.2285	.917	.2285	.921	.2285	.921	.2285	.921	.2285	.930
.2535	.932	.2535	.935	.2535	.936	.2535	.938	.2535	.938	.2535	.939	.2535	.947
.2785	.948	.2785	.952	.2785	.953	.2785	.954	.2785	.956	.2785	.955	.2785	.963
.3035	.962	.3035	.966	.3035	.967	.3035	.969	.3035	.970	.3025	.969	.3035	.975
.3285	.975	.3285	.978	.3285	.978	.3285	.979	.3285	.980	.3285	.980	.3285	.985
.3535	.985	.3535	.987	.3535	.987	.3535	.988	.3535	.988	.3535	.988	.3535	.991
.3785	.992	.3785	.993	.3785	.993	.3785	.993	.3785	.994	.3785	.993	.3785	.996
.4035	.996	.4035	.997	.4035	.996	.4035	.996	.4035	.997	.4035	.996	.4035	.998
.4285	.998	.4285	.999	.4285	.998	.4285	.998	.4285	.998	.4285	.998	.4285	.999
.4535	.999	.4535	.999	.4535	.998	.4535	.998	.4535	.999	.4535	.998	.4535	.999
		.4785	1.000	.4785	.999	.4785	.998	.4785	.999	.4785	.998	.4785	.999
				.5035	.999	.5035	.999	.5035	.999				
								.5285	.999				
								.5535	.999				
								.5785	.999				

TABLE I.—MEASURED BOUNDARY-LAYER VELOCITY PROFILES—Continued

(c) x = 39.75 inches

$R_x \times 10^{-6}$	4.91		5.55		5.96		6.36		6.78		6.74		8.31		9.56	
$p_{t\infty}$ (psia)	14.79		14.79		14.87		14.80		14.90		28.72		29.03		29.26	
T (°F)	71		64		73		77		79		69		73		77	
M	0.217		0.243		0.267		0.288		0.310		0.151		0.187		0.217	
y, inch	u/V	y, inch	u/V	y, inch	u/V	y, inch	u/V	y, inch	u/V	y, inch	u/V	y, inch	u/V	y, inch	u/V
0.0035	0.401	0.0035	0.414	0.0035	0.420	0.0035	0.426	0.0035	0.434	0.0035	0.431	0.0035	0.439	0.0035	0.445
.0085	.542	.0085	.547	.0085	.552	.0085	.554	.0085	.560	.0085	.555	.0085	.564	.0085	.558
.0135	.578	.0135	.583	.0135	.587	.0135	.591	.0135	.593	.0135	.590	.0135	.600	.0135	.599
.0185	.599	.0185	.606	.0185	.612	.0185	.613	.0185	.618	.0185	.613	.0185	.623	.0185	.626
.0235	.617	.0235	.622	.0235	.629	.0235	.631	.0235	.635	.0235	.634	.0235	.643	.0235	.647
.0285	.633	.0285	.637	.0285	.645	.0285	.647	.0285	.649	.0285	.645	.0285	.657	.0285	.661
.0335	.646	.0335	.650	.0335	.655	.0335	.659	.0335	.661	.0335	.658	.0335	.669	.0335	.674
.0385	.655	.0385	.661	.0385	.664	.0385	.670	.0385	.673	.0385	.672	.0385	.680	.0385	.685
.0435	.664	.0435	.671	.0435	.675	.0435	.679	.0435	.682	.0435	.682	.0435	.689	.0435	.695
.0485	.672	.0485	.679	.0485	.684	.0485	.688	.0485	.691	.0485	.690	.0485	.697	.0485	.703
.0535	.681	.0535	.687	.0535	.692	.0535	.695	.0545	.698	.0535	.697	.0535	.706	.0535	.712
.0785	.715	.0785	.720	.0785	.726	.0785	.730	.0635	.713	.0785	.730	.0785	.739	.0785	.744
.1035	.743	.1035	.747	.1035	.750	.1035	.755	.0735	.725	.1035	.755	.1035	.764	.1035	.768
.1285	.766	.1285	.769	.1285	.773	.1285	.777	.0835	.737	.1285	.782	.1285	.785	.1285	.791
.1535	.784	.1535	.790	.1535	.794	.1535	.798	.0935	.748	.1535	.801	.1535	.807	.1535	.810
.1785	.803	.1785	.809	.1785	.812	.1785	.816	.1035	.757	.1785	.822	.1785	.825	.1785	.829
.2035	.822	.2035	.828	.2035	.831	.2035	.834	.1235	.775	.2035	.836	.2035	.842	.2035	.846
.2535	.857	.2535	.861	.2535	.865	.2535	.869	.1435	.792	.2535	.871	.2535	.876	.2535	.879
.3035	.887	.3035	.891	.3035	.896	.3035	.898	.1635	.807	.3035	.899	.3035	.905	.3035	.909
.3535	.915	.3535	.919	.3535	.923	.3535	.927	.1835	.823	.3535	.926	.3535	.931	.3535	.936
.4035	.941	.4035	.945	.4035	.947	.4035	.950	.2035	.836	.4035	.952	.4035	.954	.4035	.957
.4535	.960	.4535	.964	.4535	.968	.4535	.971	.2235	.850	.4535	.971	.4535	.974	.4535	.976
.5035	.978	.5035	.981	.5035	.983	.5035	.985	.2435	.863	.5035	.989	.5035	.987	.5035	.989
.5535	.990	.5535	.991	.5535	.993	.5535	.994	.2635	.877	.5535	.994	.5535	.995	.5535	.995
.6035	.996	.6035	.996	.6035	.996	.6035	.998	.2835	.889	.6035	.998	.6035	.997	.6035	.998
.6535	.998	.6535	.998	.6535	.999	.6535	.999	.3035	.901					.6535	.999
.7035	.999	.7035	.998	.7035	.999	.7035	1.000	.3235	.911						
.7535	.999	.7535	.998			.7535	1.000	.3435	.922						
.8035	.999	.8035	.998					.3635	.933						
		.8535	.998					.3835	.942						
								.4035	.951						
								.4235	.960						
								.4435	.968						
								.4635	.975						
								.4835	.980						
								.5035	.985						
								.5235	.990						
								.5435	.993						
								.5635	.995						
								.5835	.996						
								.6035	.998						
								.6235	.998						
								.6435	.999						
								.6635	.999						

TABLE I.—MEASURED BOUNDARY-LAYER VELOCITY PROFILES—Continued

(c) $x=39.75$ inches—Continued

$R_x \times 10^{-6}$	10.68	12.53		13.45		12.55		17.34		21.29		25.82		26.21	
$p_{t\infty}$ (psia)	29.75	30.35		30.55		73.39		74.57		75.87		78.80		78.34	
T (°F)	85	93		94		69		75		81		83		100	
M	0.244	0.290		0.311		0.108		0.152		0.187		0.221		0.235	
y, inch	u/V	y, inch	u/V	y, inch	u/V	y, inch	u/V	y, inch	u/V	y, inch	u/V	y, inch	u/V	y, inch	u/V
0.0035	0.450	0.0035	0.455	0.0035	0.460	0.0035	0.455	0.0035	0.469	0.0035	0.520	0.0035	0.488	0.0035	0.493
.0085	.562	.0085	.570	.0085	.555	.0085	.568	.0085	.588	.0085	.610	.0085	.603	.0085	.603
.0135	.605	.0135	.613	.0135	.614	.0135	.612	.0135	.630	.0135	.645	.0135	.645	.0135	.645
.0185	.632	.0185	.639	.0185	.642	.0185	.638	.0185	.656	.0185	.648	.0185	.668	.0185	.669
.0235	.652	.0235	.659	.0235	.663	.0235	.658	.0285	.688	.0235	.684	.0235	.686	.0235	.688
.0285	.667	.0285	.674	.0285	.678	.0285	.673	.0335	.701	.0285	.699	.0285	.700	.0285	.701
.0335	.679	.0335	.686	.0335	.689	.0335	.685	.0385	.711	.0335	.709	.0333	.712	.0335	.713
.0385	.691	.0385	.696	.0385	.700	.0385	.697	.0435	.720	.0385	.720	.0385	.723	.0385	.722
.0435	.700	.0435	.707	.0435	.708	.0435	.706	.0485	.728	.0435	.728	.0435	.730	.0435	.730
.0485	.709	.0485	.715	.0485	.717	.0485	.714	.0535	.735	.0485	.735	.0485	.738	.0485	.739
.0535	.717	.0535	.722	.0535	.725	.0535	.722	.0785	.766	.0535	.742	.0535	.746	.0535	.746
.0785	.747	.0785	.753	.0785	.756	.0785	.754	.1035	.789	.0635	.756	.0635	.758	.0635	.758
.1035	.773	.1035	.778	.1035	.781	.1035	.777	.1285	.809	.0735	.768	.0735	.769	.0735	.770
.1285	.795	.1285	.799	.1285	.802	.1285	.798	.1535	.829	.0835	.777	.0835	.779	.0835	.780
.1535	.811	.1535	.818	.1535	.821	.1535	.817	.1785	.817	.0935	.787	.0935	.788	.0935	.789
.1785	.833	.1785	.836	.1785	.839	.1785	.837	.2035	.863	.1035	.796	.1035	.797	.1035	.799
.2285		.2285		.2285		.2285		.2335	.894	.1285	.815	.1285	.811	.1285	.817
.2535	.882	.2535	.886	.2535	.873	.2535	.870	.3035	.921	.1535	.834	.1535	.835	.1535	.836
.3035	.911	.3035	.914	.3035	.889	.3035	.886	.3535	.946	.1785	.852	.1785	.853	.1785	.854
.3535	.938	.3535	.940	.3535	.916	.3535	.914	.4035	.967	.2035	.869	.2035	.870	.2035	.871
.4035	.960	.4035	.963	.4035	.941	.4035	.941	.4535	.983	.2535	.899	.2535	.900	.2535	.900
.4535	.978	.4535	.979	.4535	.964	.4535	.962	.5035	.993	.3035	.926	.3035	.927	.3035	.928
.5035	.990	.5035	.991	.5035	.980	.5035	.980	.5535	.998	.3535	.949	.3535	.952	.3535	.951
.5535	.996	.5535	.997	.5535	.991	.5535	.991	.6035	.999	.4035	.971	.4035	.970	.4035	.970
.6035	.999	.6035	.999	.6035	.997	.6035	.998			.4535	.984	.4535	.983	.4535	.985
.6535	.999	.6535	.999	.6535	.999	.6535	1.000			.5035	.995	.5035	.993	.5035	.993
					1.000		1.000			.5535	.999	.5535	.997	.5535	.997
										.6035	1.000	.6035	.997	.6035	.997
										.6535	1.000	.6535	.998	.6535	.998
												.7035	.998	.7035	.998
												.7535	.998		

TABLE I. MEASURED BOUNDARY-LAYER
VELOCITY PROFILES –Continued

(e) $x = 39.75$ inches Concluded

$P_x \times 10^{-6}$	30.29		28.86		28.11	
p_{t_∞} (psia)	80.51		79.82		78.22	
T (°F)	107		108		90	
M	0.272		0.260		0.247	
y, inch	u/V	y, inch	u/V	y, inch	u/V
0.0035	0.509	0.0035	0.511	0.0035	0.488
.0085	.614	.0085	.614	.0085	.609
.0135	.653	.0135	.652	.0135	648
.0185	.676	.0185	.675	.0185	.671
.0235	.694	.0235	.692	.0235	.690
.0285	.708	.0285	.705	.0285	.704
.0335	.720	.0335	.718	.0335	.716
.0385	.728	.0385	.727	.0385	.725
.0435	.738	.0435	.736	.0435	.734
.0485	.744	.0485	.744	.0485	.741
.0535	.751	.0535	.751	.0535	.749
.0585	.756	.0635	.763	.0635	.760
.0635	.763	.0735	.773	.0735	.771
.0735	.774	.0835	.783	.0835	.781
.0835	.784	.0935	.792	.0935	.791
.0935	.792	.1035	.801	.1035	.799
.1035	.801	.1285	.821	.1285	.820
.1285	.821	.1535	.840	.1535	.839
.1535	.841	.1785	.858	.1785	.855
.1785	.858	.2035	.873	.2035	.872
.2035	.874	.2535	.904	.2535	.902
.2535	.903	.3035	.930	.3035	.929
.3035	.931	.3535	.956	.3535	.953
.3535	.955	.4035	.974	.4035	.972
.4035	.973	.4535	.987	.4535	.986
.4535	.987	.5035	.996	.5035	.993
.5035	.995	.5535	.999	.5535	.997
.5535	.998	.6035	1.000	.6035	.998
.6035	.999	.6535	1.000	.6535	.998
.6535	.999	.7035	1.000	.7035	.998
.7035	.999	.7535	1.000	.7535	.998
.7535	.999	.8035	1.000		
.8035	.999				
.8535	.999				
.9035	.999				

TABLE I.—MEASURED BOUNDARY-LAYER VELOCITY PROFILES—Continued

(d) x=51.75 inches

$P_t \times 10^{-6}=4.78$, p_∞ (psia) $=7.97$, T (°F) $=81$, $M=0.317$

y, inch	u/V
0.0035	0.336
.0085	.497
.0135	.542
.0185	.569
.0235	.589
.0285	.600
.0335	.611
.0385	.623
.0435	.633
.0485	.640
.0535	.648
.0785	.680
.1035	.705
.1285	.725
.1535	.745
.1785	.761
.2035	.77
.2535	.806
.3035	.833
.3535	.861
.4035	.885
.4535	.907
.5035	.927
.5535	.945
.6035	.963
.6535	.976
.7035	.984
.7535	.992
.8035	.994
.8535	.996
.9035	.998
.9535	.998
1.0035	.998
1.0535	1.000

$P_t \times 10^{-6}=6.46$, $p_\infty=14.84$, $T=73$, $M=0.221$

y, inch	u/V
0.0035	0.390
.0085	.524
.0135	.566
.0185	.586
.0235	.604
.0285	.619
.0335	.633
.0385	.644
.0435	.653
.0485	.663
.0535	.668
.0785	.702
.1035	.728
.1285	.748
.1535	.765
.1785	.780
.2035	.797
.2535	.827
.3035	.853
.3535	.876
.4035	.899
.4535	.92
.5035	.942
.5535	.958
.6035	.970
.6535	.983
.7035	.992
.7535	.996
.8035	.998
.8535	1.000

$P_t \times 10^{-6}=7.16$, $p_\infty=14.89$, $T=80$, $M=0.248$

y, inch	u/V
0.0035	0.386
.0085	.527
.0135	.568
.0185	.591
.0235	.609
.0285	.624
.0335	.637
.0385	.645
.0435	.657
.0485	.668
.0535	.674
.0785	.707
.1035	.732
.1285	.751
.1535	.768
.2035	.800
.2535	.832
.3035	.857
.3535	.882
.4035	.905
.4535	.925
.5035	.94
.5535	.961
.6035	.973
.6535	.986
.7035	.991
.7535	.997
.8035	.999
.8535	.999
.9035	1.000

$P_t \times 10^{-6}=7.92$, $p_\infty=14.90$, $T=76$, $M=0.274$

y, inch	u/V
0.0035	0.389
.0085	.535
.0135	.572
.0185	.598
.0235	.616
.0285	.632
.0335	.643
.0385	.652
.0435	.663
.0485	.672
.0535	.680
.0785	.711
.1035	.734
.1285	.756
.1535	.775
.1785	.790
.2285	.821
.2785	.847
.3285	.874
.3785	.896
.4285	.918
.4785	.93
.5285	.956
.5785	.970
.6285	.982
.6785	.991
.7285	.996
.7785	.998
.8285	.999
.8785	.999

$P_t \times 10^{-6}=8.52$, $p_\infty=15.13$, $T=81$, $M=0.295$

y, inch	u/V
0.0035	0.406
.0085	.540
.0135	.576
.0185	.600
.0235	.615
.0285	.634
.0335	.644
.0385	.657
.0435	.666
.0485	.673
.0535	.681
.0785	.714
.1035	.740
.1285	.760
.1535	.777
.1785	.794
.2035	.809
.2535	.836
.3035	.863
.3535	.888
.4035	.909
.4525	.929
.4785	.949
.5035	.958
.5285	.965
.5535	.972
.5785	.977
.6035	.984
.6285	.988
.6535	.992
.6785	.994
.7035	.996
.7285	.998
.7535	.999
.7785	

$P_t \times 10^{-6}=9.05$, $p_\infty=15.20$, $T=85$, $M=0.317$

y, inch	u/V
0.0035	0.409
.0085	.543
.0135	.579
.0185	.602
.0235	.620
.0285	.635
.0335	.647
.0385	.658
.0435	.669
.0485	.678
.0535	.686
.0785	.717
.1035	.741
.1285	.762
.1535	.778
.1785	.796
.2035	.810
.2285	.824
.2535	.837
.2785	.851
.3035	.866
.3535	.87
.3785	.888
.4035	.901
.4285	.920
.4545	.931
.4785	.941
.5035	.950
.5285	.959
.5535	.966
.5785	.974
.6035	.978
.6285	.983
.6535	.988
.6785	.993
.7035	.994
.7285	.996
.7535	.997
.7785	.998
.8035	.999

$P_t \times 10^{-6}=8.96$, $p_\infty=29.66$, $T=83$, $M=0.155$

y, inch	u/V
0.0035	0.428
.0085	.538
.0135	.581
.0185	.604
.0235	.622
.0285	.638
.0335	.648
.0385	.660
.0435	.671
.0485	.680
.0535	.688
.0785	.718
.1035	.743
.1285	.762
.1535	.779
.1785	.797
.2035	.813
.2535	.841
.3035	.867
.3535	.880
.4035	.912
.4535	.93
.5035	.951
.5535	.967
.6035	.980
.6535	.990
.7035	.995
.7535	1.000

$P_t \times 10^{-6}=10.95$, $p_\infty=29.81$, $T=86$, $M=0.190$

y, inch	u/V
0.0035	0.430
.0085	.553
.0135	.589
.0185	.611
.0235	.630
.0285	.645
.0335	.658
.0385	.668
.0435	.677
.0485	.686
.0535	.695
.0785	.724
.1035	.748
.1285	.769
.1535	.785
.1785	.802
.2035	.816
.2535	.843
.3035	.870
.3535	.894
.4035	.915
.4535	.931
.5035	.953
.5535	.968
.6035	.981
.6535	.989
.7035	.996
.7535	.999
.8035	.999
.8535	1.000

TABLE I.—MEASURED BOUNDARY-LAYER VELOCITY PROFILES—Continued

(d) x=51.75 inches Continued

$R_x \times 10^{-6}$	12.55		14.09		15.54		16.61		16.94		18.89		26.75		30.55	
$p_{t\infty}$ (psia)	30.00		29.66		29.56		29.76		29.47		84.01		85.15		80.49	
T (°F)	91		85		79		86		88		67		71		77	
M	0.221		0.249		0.273		0.295		0.319		0.111		0.157		0.193	
y, inch	u/V	y, inch	u/V	y, inch	u/V	y, inch	u/V	y, inch	u/V	y, inch	u/V	y, inch	u/V	y, inch	u/V
0.0035	0.431	0.0035	0.442	0.0035	0.450	0.0035	0.458	0.0035	0.429	0.0035	0.445	0.0035	0.458	0.0035	0.457
.0085	.557	.0085	.565	.0085	.569	.0085	.573	.0085	.466	.0085	.568	.0085	.582	.0085	.589
.0135	.595	.0135	.598	.0135	.607	.0135	.609	.0135	.575	.0135	.608	.0135	.621	.0135	.631
.0185	.619	.0185	.626	.0185	.631	.0185	.634	.0185	.612	.0185	.632	.0185	.652	.0185	.656
.0235	.635	.0235	.641	.0235	.648	.0235	.652	.0235	.636	.0235	.655	.0235	.669	.0235	.675
.0285	.652	.0285	.658	.0285	.663	.0285	.665	.0285	.654	.0285	.669	.0285	.683	.0285	.688
.0335	.664	.0335	.669	.0335	.675	.0335	.678	.0335	.668	.0335	.681	.0335	.695	.0335	.699
.0385	.675	.0385	.678	.0385	.685	.0385	.687	.0385	.680	.0385	.689	.0385	.705	.0385	.709
.0435	.684	.0435	.688	.0435	.694	.0435	.698	.0435	.691	.0435	.701	.0435	.713	.0435	.718
.0485	.694	.0485	.698	.0485	.702	.0485	.705	.0485	.699	.0485	.708	.0485	.720	.0485	.724
.0535	.701	.0535	.704	.0535	.711	.0535	.712	.0535	.706	.0535	.716	.0535	.727	.0535	.731
.0785	.732	.0785	.735	.0785	.740	.0785	.743	.0785	.737	.0785	.745	.0785	.756	.0785	.760
.1035	.755	.1035	.757	.1035	.760	.1035	.765	.1035	.761	.1035	.766	.1035	.777	.1035	.781
.1285	.774	.1285	.777	.1285	.781	.1285	.782	.1285	.779	.1285	.787	.1285	.796	.1285	.800
.1535	.791	.1535	.794	.1535	.794	.1535	.800	.1535	.797	.1535	.803	.1535	.813	.1535	.815
.1785	.806	.1785	.809			.1785	.815	.1785	.812	.1785	.816	.1785	.827	.1785	.830
.2035	.821	.2035	.824	.2035	.827	.2035	.829	.2035	.827	.2035	.829	.2035	.841	.2035	.844
.2535	.849	.2535	.850	.2535	.855	.2535	.856	.2535	.854	.2535	.857	.2535	.868	.2535	.871
.3035	.874	.3035	.876	.3035	.878	.3035	.882	.3035	.879	.3035	.882	.3035	.890	.3035	.895
.3535	.897	.3535	.900	.3535	.902	.3535	.908	.3535	.902	.3535	.903	.3535	.913	.3535	.915
.4035	.920	.4035	.921	.4035	.921	.4035	.925	.4035	.923	.4035	.924	.4035	.932	.4035	.936
.4535	.940	.4535	.940	.4535	.943	.4535	.943	.4535	.941	.4535	.944	.4535	.951	.4535	.953
.5035	.957	.5035	.957	.5035	.961	.5035	.962	.5035	.960	.5035	.961	.5035	.967	.5035	.969
.5535	.971	.5535	.972	.5535	.973	.5535	.975	.5535	.973	.5535	.975	.5535	.980	.5535	.982
.6035	.983	.6035	.984	.6035	.984	.6035	.986	.6035	.984	.6035	.986	.6035	.989	.6035	.991
.6535	.991	.6535	.992	.6535	.991	.6535	.993	.6535	.992	.6535	.992	.6535	.996	.6535	.996
.7035	.996	.7035	.996	.7035	.996	.7035	.997	.7035	.996	.7035	.996	.7035	.998	.7035	.999
.7535	.998	.7535	.998	.7535	.998	.7535	.999	.7535	.999	.7535	.998	.7535	.999	.7535	1.000
.8035	.999	.8035	.999	.8035	1.000	.8035	.999	.8035	.999	.8035	.999	.8035	1.000	.8035	1.000
.8535	1.000	.8535	.999			.8535	.999	.8535	1.000			.8535	1.000	.8535	1.000
		.9035	.999					.9035	1.000			.9035	1.000		
								.9535	1.000			.9535	1.000		
								1.0035	1.000						
								1.0535	1.000						

TABLE I.—MEASURED BOUNDARY-LAYER VELOCITY PROFILES—Concluded

(d) $x = 51.75$ inches—Concluded

$R_x \times 10^{-6}$	32.54		34.78		36.82		39.32		41.24	
$p_{t,x}$ (psia)	76.25		78.02		80.29		81.69		80.84	
T (°F)	89		95		104		108		94	
M	0.224		0.238		0.251		0.263		0.275	
y, inch	u/V	y, inch	u/V	y, inch	u/V	y, inch	u/V	y, inch	u/V
0.0035	0.483	0.0035	0.489	0.0035	0.495	0.0035	0.500	0.0035	0.512
.0085	.589	.0085	.594	.0085	.597	.0085	.602	.0085	.607
.0135	.631	.0135	.633	.0135	.636	.0135	.639	.0135	.643
.0185	.655	.0185	.658	.0185	.658	.0185	.663	.0185	.667
.0235	.673	.0235	.675	.0235	.675	.0235	.680	.0235	.684
.0285	.687	.0285	.689	.0285	.691	.0285	.693	.0285	.697
.0335	.698	.0335	.701	.0335	.702	.0335	.704	.0335	.709
.0385	.709	.0385	.711	.0385	.712	.0385	.713	.0385	.718
.0435	.717	.0435	.719	.0435	.722	.0435	.722	.0435	.728
.0485	.725	.0485	.726	.0485	.729	.0485	.730	.0485	.733
.0535	.732	.0535	.733	.0535	.735	.0535	.737	.0535	.740
.0635	.743	.0635	.745	.0635	.747	.0635	.748	.0635	.751
.0735	.754	.0735	.755	.0735	.756	.0735	.757	.0735	.760
.0835	.764	.0835	.764	.0835	.766	.0835	.767	.0835	.770
.0935	.772	.0935	.773	.0935	.775	.0935	.775	.0935	.778
.1035	.780	.1035	.781	.1035	.782	.1035	.783	.1035	.786
.1285	.798	.1285	.799	.1285	.800	.1285	.800	.1285	.802
.1535	.813	.1535	.815	.1535	.817	.1535	.818	.1535	.820
.1785	.828	.1785	.829	.1785	.832	.1785	.832	.1785	.833
.2035	.842	.2035	.843	.2035	.845	.2035	.847	.2035	.849
.2535	.869	.2535	.870	.2535	.870	.2535	.872	.2535	.875
.3035	.892	.3035	.893	.3035	.894	.3035	.895	.3035	.898
.3535	.914	.3535	.915	.3535	.916	.3535	.916	.3535	.919
.4035	.935	.4035	.935	.4035	.936	.4035	.937	.4035	.938
.4535	.951	.4535	.952	.4535	.955	.4535	.954	.4535	.957
.5035	.966	.5035	.967	.5035	.968	.5035	.969	.5035	.972
.5535	.979	.5535	.980	.5535	.981	.5535	.980	.5535	.983
.6035	.989	.6035	.989	.6035	.989	.6035	.990	.6035	.991
.6535	.994	.6535	.994	.6535	.994	.6535	.994	.6535	.996
.7035	.996	.7035	.996	.7035	.997	.7035	.997	.7035	.998
.7535	.997	.7535	.997	.7535	.998			.7535	.999
.8035	.998	.8035	.997	.8035	.998			.8035	.999
.8535	.998	.8535	.998					.8535	.999
.9035	.998								

TABLE II.—MEASURED LOCAL SKIN-FRICTION COEFFICIENT

(a) r = 18.00 inches

$p_{l\infty}$ (psia) 7.55

M	$P_x \times 10^{-6}$	$c_f \times 10^3$
0.229	1.24	3.75
.249	1.35	3.59
.275	1.48	3.43
.295	1.58	3.38
.317	1.68	3.32
.221	1.20	3.63
.249	1.34	3.60
.274	1.47	3.44
.296	1.59	3.47
.315	1.67	3.34
.224	1.21	3.64
.252	1.36	3.57
.272	1.45	3.43
.296	1.58	3.33
.318	1.69	3.32

$p_{l\infty}$ = 15.15

M	$P_x \times 10^{-6}$	$c_f \times 10^3$
0.225	2.39	3.18
.247	2.60	3.09
.270	2.84	3.03
.292	3.07	2.99
.314	3.27	2.92
.220	2.33	3.15
.246	2.59	3.08
.269	2.82	3.01
.291	3.05	2.98
.313	3.26	2.91
.219	2.32	3.07
.247	2.60	3.10
.269	2.82	2.99
.292	3.05	2.98
.314	3.26	2.91

$p_{l\infty}$ = 29.99

M	$P_x \times 10^{-6}$	$c_f \times 10^3$
0.153	3.17	3.02
.187	3.83	2.84
.219	4.52	2.76
.246	5.03	2.75
.269	5.47	2.68
.290	5.85	2.65
.311	6.25	2.60
.156	3.24	2.95
.189	3.88	2.85
.220	4.54	2.80
.246	5.07	2.73
.270	5.46	2.71
.291	5.87	2.67
.312	6.22	2.62
.155	3.21	2.90
.187	3.87	2.83
.218	4.50	2.77
.246	5.05	2.74
.268	5.50	2.70
.290	5.85	2.67
.311	6.25	2.64

$p_{l\infty}$ = 48.81

M	$P_x \times 10^{-6}$	$c_f \times 10^3$
0.107	3.73	2.85
.153	5.31	2.71
.188	6.39	2.63
.217	7.42	2.57
.109	3.79	2.88
.152	5.32	2.63
.187	6.44	2.62
.218	7.43	2.56
.107	3.71	2.90
.152	5.31	2.70
.187	6.44	2.61
.217	7.40	2.58

$p_{l\infty}$ = 67.26

M	$P_x \times 10^{-6}$	$c_f \times 10^3$
0.108	5.20	2.78
.153	7.35	2.63
.188	8.99	2.52
.108	5.21	2.74
.153	7.34	2.60
.188	8.96	2.50
.108	5.20	2.64
.153	7.33	2.58
.188	8.95	2.53

$p_{l\infty}$ (psia) 75.28

M	$P_x \times 10^{-6}$	$c_f \times 10^3$
0.108	5.88	2.73
.153	8.29	2.58
.188	10.09	2.48
.108	5.84	2.68
.153	8.26	2.57
.188	10.11	2.50
.108	5.84	2.72
.154	8.28	2.56
.188	10.05	2.45

TABLE II.—MEASURED LOCAL SKIN-FRICTION COEFFICIENT—Continued

(b) $x = 30.00$ inches

$p_{t,\infty}$ (psia) 7.68

M	$R_x \times 10^{-6}$	$c_f \times 10^3$
0.223	2.04	3.25
.247	2.24	3.20
.276	2.50	3.11
.299	2.69	3.09
.316	2.82	3.05
.219	1.99	3.18
.253	2.29	3.20
.272	2.46	3.13
.295	2.65	3.09
.319	2.84	3.03
.220	2.01	3.24
.250	2.27	3.13
.274	2.48	3.13
.300	2.70	3.07
.316	2.83	3.04

14.90

M	$R_x \times 10^{-6}$	$c_f \times 10^3$
0.218	3.90	2.76
.245	4.33	2.74
.268	4.72	2.74
.290	5.04	2.75
.313	5.39	2.73
.218	3.84	2.81
.245	4.30	2.77
.269	4.67	2.75
.291	5.01	2.74
.313	5.37	2.69
.218	3.86	2.86
.245	4.27	2.79
.268	4.66	2.73
.290	4.99	2.71
.313	5.86	2.71

15.14

M	$R_x \times 10^{-6}$	$c_f \times 10^3$
0.223	3.97	2.93
.247	4.41	2.83
.272	4.83	2.80
.292	5.15	2.74
.315	5.52	2.72
.220	3.92	2.84
.247	4.36	2.82
.271	4.78	2.80
.293	5.16	2.76
.312	5.46	2.70
.219	3.89	2.86
.246	4.35	2.83
.272	4.81	2.77
.292	5.15	2.72
.313	5.46	2.69

28.55

M	$R_x \times 10^{-6}$	$c_f \times 10^3$
0.312	9.93	2.46
.291	9.35	2.48
.269	8.67	2.53
.244	7.89	2.54
.217	7.05	2.57
.188	6.15	2.62
.153	5.03	2.63
.312	9.95	2.46
.292	9.37	2.49
.268	8.65	2.50
.244	7.90	2.54
.217	7.05	2.56
.188	6.15	2.58
.153	5.05	2.65

48.41

M	$R_x \times 10^{-6}$	$c_f \times 10^3$
0.110	6.37	------
.153	8.84	2.60
.189	10.83	2.50
.218	12.44	2.45
.109	6.28	2.58
.154	8.86	2.55
.190	10.87	2.50
.218	12.40	2.45
.109	6.28	2.57
.154	8.83	2.57
.188	10.76	2.50
.218	12.34	2.44

$p_{t,\infty}$ (psia) 67.49

M	$R_x \times 10^{-6}$	$c_f \times 10^3$
0.218	17.59	2.34
.188	15.30	2.36
.154	12.56	2.39
.108	8.83	------
.219	17.63	2.32
.188	15.26	2.33
.153	12.54	2.37
.107	8.78	2.45

77.67

M	$R_x \times 10^{-6}$	$c_f \times 10^3$
0.110	10.18	2.51
.155	14.14	2.43
.188	16.98	2.35
.110	10.01	2.47
.154	13.99	2.43
.188	16.98	2.33
.110	10.01	2.37
.155	14.05	2.45
.189	17.00	------

TABLE II.—MEASURED LOCAL SKIN-FRICTION COEFFICIENT—Continued

(c) $x = 42.00$ inches

$p_{t\infty}$ (psia) 7.76			7.77			15.10			15.01			28.94		
M	$P_z\times10^{-6}$	$C_f\times10^3$	M	$P_z\times10^{-6}$	$C_f\times10^3$	M	$P_z\times10^{-6}$	$C_f\times10^3$	M	$P_z\times10^{-6}$	$C_f\times10^3$	M	$P_z\times10^{-6}$	$C_f\times10^3$
0.225	2.90	3.01	0.225	2.85	3.09	0.244	6.03	2.70	0.217	5.36	2.63	0.156	7.36	02.55
.249	3.20	2.83	.276	3.48	2.91	.218	5.41	2.69	.244	5.98	2.60	.190	8.97	2.51
.272	3.48	2.91	.317	3.96	2.88	.269	6.62	2.67	.268	6.50	2.57	.220	10.36	2.49
.300	3.82	2.83	.248	3.15	2.86	.293	7.17	2.60	.289	7.00	2.58	.247	11.54	2.48
.316	4.01	2.80	.297	3.71	2.89	.313	7.64	2.58	.311	7.46	2.53	.271	12.59	2.44
.215	2.78	2.99	.221	2.82	2.90	.218	5.41	2.69	.218	5.32	2.53	.292	13.49	2.43
.254	3.26	2.83	.250	3.17	2.90	.244	6.03	2.67	.244	5.95	2.58	.314	14.36	2.41
.274	3.50	2.94	.273	3.46	2.95	.268	6.58	2.62	.267	6.48	2.54	.154	7.28	2.63
.294	3.75	2.84	.297	3.72	2.86	.291	7.12	2.60	.291	7.02	2.56	.190	8.96	2.52
.318	4.02		.314	3.92	2.82	.313	7.65	2.57	.312	7.46	2.54	.220	10.29	2.47
.223	2.88	2.94	.222	2.83	3.07	.221	5.46	2.62	.218	5.30	2.61	.247	11.48	2.47
.252	3.24	2.86	.250	3.17	3.01	.245	6.04	2.65	.246	5.94	2.58	.271	12.58	2.45
.276	3.52	2.91	.273	3.45	2.97	.269	6.61	2.62	.268	6.49	2.62	.293	13.50	2.41
.297	3.78	2.83	.296	3.72	2.85	.292	7.14	2.60	.291	7.00	2.56	.313	14.21	2.37
.315	3.99	2.82	.316	3.95	2.82	.314	7.62	2.59	.312	7.45	2.53			

$p_{t\infty}$ (psia) 29.29			48.25			67.59			75.19			79.27		
M	$P_z\times10^{-6}$	$C_f\times10^3$	M	$P_z\times10^{-6}$	$C_f\times10^3$	M	$P_z\times10^{-6}$	$C_f\times10^3$	M	$P_z\times10^{-6}$	$C_f\times10^3$	M	$P_z\times10^{-6}$	$C_f\times10^3$
0.313	14.49	2.35	0.109	8.84		0.108	12.22	2.41	0.109	13.78	2.44	0.275	33.54	2.19
.292	13.59	2.37	.153	12.31	2.44	.154	17.28	2.32	.153	19.30	2.29	.269	32.77	2.18
.269	12.64	2.38	.188	15.03	2.37	.188	21.04	2.27	.188	23.50	2.22	.258	31.42	2.18
.245	11.51	2.41	.218	17.34	2.36	.108	12.17		.108	13.52	2.42	.245	30.04	2.19
.218	10.31	2.40	.108	8.79	2.52	.154	17.36	2.30	.153	19.29	2.28	.232	28.67	2.21
.188	9.06	2.46	.153	12.30	2.43	.188	21.09	2.26	.188	23.47	2.20	.219	26.98	2.22
.154	7.41	2.48	.188	15.02	2.39	.108	12.22	2.42	.108	13.57	2.39	.189	23.45	2.25
.313	14.46	2.36	.218	17.32	2.33	.153	17.38	2.28	.153	19.25	2.25	.153	19.18	2.30
.292	13.54	2.37	.108	8.76	2.54	.189	21.18	2.27	.188	23.42	2.22	.109	13.61	2.33
.269	12.61	2.37	.153	12.28	2.43							.276	33.76	2.17
.245	11.54	2.40	.188	15.02	2.38							.270	32.94	2.15
.219	10.31	2.43	.218	17.32	2.36							.258	31.43	2.17
.188	9.00	2.42										.245	29.97	2.19
.153	7.31	2.50										.232	28.58	2.17
.314	14.52	2.36										.219	26.88	2.20
.292	13.62	2.39										.189	23.55	2.25
.269	12.67	2.37										.153	19.10	2.29
.244	11.46	2.38										.108	13.54	2.38
.218	10.31	2.42										.277	33.73	2.15
.188	8.98	2.41										.270	32.92	2.16
.152	7.25	2.44										.258	31.44	2.18
												.246	29.94	2.19
												.232	28.54	2.19
												.219	26.85	2.21
												.189	23.39	2.23
												.154	19.09	2.30
												.109	13.64	2.38

TABLE II. MEASURED LOCAL SKIN-FRICTION COEFFICIENT—Concluded

(d) $x = 54.00$ inches

$p_{t,\infty}$ (psia) 7.61			48.03			67.85			74.68			79.04		
M	$R_x \times 10^{-6}$	$c_f \times 10^3$	M	$R_x \times 10^{-6}$	$c_f \times 10^3$	M	$R_x \times 10^{-6}$	$c_f \times 10^3$	M	$R_x \times 10^{-6}$	$c_f \times 10^3$	M	$R_x \times 10^{-6}$	$c_f \times 10^3$
0.226	3.75	2.81	0.109	11.35	2.61	0.109	15.91	2.45	0.109	17.83	2.40	0.111	18.02	2.33
.254	4.20	2.74	.154	15.98	2.39	.155	22.67	2.28	.154	25.18	2.24	.156	25.24	2.21
.277	4.54	2.75	.189	19.46	2.32	.189	27.45	2.21	.189	30.48	2.17	.190	30.60	2.17
.300	4.89	2.74	.219	22.45	2.28	.108	16.05	2.41	.109	15.83	---	.220	35.16	2.13
.319	5.17	2.72	.109	11.32	2.58	.152	22.48	2.28	.154	25.12	---	.233	37.15	2.12
.224	3.71	2.78	.154	15.95	2.40	.189	27.45	2.21	.189	30.52	2.16	.247	39.18	2.09
.251	4.12	2.78	.189	19.48	2.31	.109	15.93	2.43	.109	17.81	2.33	.261	41.10	2.10
.274	4.52	2.73	.218	22.32	2.28	.154	22.48	2.25	.154	25.08	2.24	.273	42.83	2.08
.300	4.89	2.79	.108	11.22	2.50	.189	27.35	2.20	.189	30.50	2.17	.276	43.25	2.08
.319	5.16	2.73	.154	15.93	2.39				.154	24.98	2.22	.111	17.80	2.38
.226	3.70	2.80	.189	19.46	2.33				.189	30.46	2.16	.156	25.11	2.26
.255	4.19	2.82	.218	22.32	2.27							.191	30.51	2.20
.277	4.53	2.73										.221	35.14	2.13
.297	4.86	2.73										.234	37.04	2.13
.320	5.19	2.75										.247	38.98	2.12
												.250	40.83	2.28
												.272	42.31	2.08
												.277	42.98	2.08
												.111	17.69	2.45
												.156	25.01	2.27
												.191	30.45	2.21
												.220	34.89	2.17
												.233	36.79	2.16
												.247	38.90	2.12
												.259	40.56	2.12
												.273	42.55	2.11
												.278	42.34	2.09

TABLE III.—SUMMARY OF MAJOR PARAMETERS OBTAINED FROM MEASURED BOUNDARY-LAYER PROFILES

r, in.	M	$p_{t\infty}$ psia	$P_x \times 10^{-6}$	θ, in.	δ^*, in.	δ, in.	$\dfrac{\delta^*}{\theta}$	C_f
15.75	0.308	7.94	1.43	0.0331	0.0456	0.296	1.378	0.00346
15.75	.215	15.17	1.97	.0305	.0424	.263	1.390	.00324
15.75	.241	14.81	2.15	.0301	.0413	.257	1.372	.00318
15.75	.264	14.83	2.33	.0291	.0401	.247	1.378	.00313
15.75	.288	14.84	2.51	.0292	.0397	.245	1.360	.00309
15.75	.307	14.86	2.64	.0288	.0395	.243	1.372	.00305
15.75	.152	28.41	2.65	.0283	.0392	.242	1.385	.00306
15.75	.187	28.65	3.24	.0276	.0387	.240	1.402	.00294
15.75	.216	28.94	3.72	.0265	.0366	.233	1.381	.00286
15.75	.243	29.25	4.16	.0262	.0360	.228	1.374	.00282
15.75	.265	29.37	4.56	.0258	.0348	.224	1.365	.00278
15.75	.289	30.73	5.13	.0251	.0344	.221	1.371	.00273
15.75	.308	30.52	5.48	.0245	.0328	.218	1.339	.00271
15.75	.107	78.45	5.18	.0247	.0340	.219	1.377	.00273
15.75	.188	78.83	8.82	.0226	.0301	.207	1.332	.00253
27.75	.309	7.77	2.52	.0535	.0733	.453	1.379	.00309
27.75	.307	8.23	2.53	.0529	.0729	.447	1.379	.00309
27.75	.307	7.93	2.53	.0518	.0722	.447	1.410	.00309
27.75	.214	14.75	3.33	.0480	.0655	.410	1.365	.00293
27.75	.216	14.87	3.26	.0483	.0665	.415	1.377	.00294
27.75	.213	15.21	3.47	.0475	.0651	.402	1.371	.00290
27.75	.242	15.01	3.83	.0476	.0650	.403	1.380	.00285
27.75	.266	15.07	4.17	.0467	.0634	.398	1.365	.00282
27.75	.288	15.01	4.50	.0457	.0621	.394	1.359	.00279
27.75	.310	14.94	4.70	.0453	.0617	.393	1.362	.00277
27.75	.309	14.94	4.62	.0461	.0619	.397	1.346	.00277
27.75	.308	14.95	4.67	.0454	.0618	.391	1.361	.00277
27.75	.152	29.51	4.90	.0438	.0596	.384	1.361	.00275
27.75	.186	29.45	5.82	.0431	.0576	.377	1.336	.00269
27.75	.217	29.46	6.74	.0416	.0561	.371	1.349	.00263
27.75	.243	29.10	7.58	.0408	.0546	.370	1.338	.00259
27.75	.242	29.97	7.56	.0413	.0561	.371	1.358	.00259
27.75	.242	29.45	7.45	.0414	.0553	.366	1.336	.00260
27.75	.266	29.62	8.09	.0408	.0544	.364	1.333	.00256
27.75	.288	30.32	9.00	.0402	.0531	.363	1.321	.00252
27.75	.310	30.63	9.60	.0395	.0525	.359	1.329	.00250
27.75	.310	30.83	9.49	.0392	.0529	.361	1.349	.00251
27.75	.309	30.11	9.21	.0398	.0532	.360	1.337	.00252
27.75	.108	85.28	10.04	.0390	.0520	.367	1.333	.00249
27.75	.152	84.93	14.08	.0370	.0485	.346	1.311	.00239
39.75	.217	14.79	4.91	.0650	.0868	.556	1.335	.00269
39.75	.243	14.79	5.55	.0630	.0840	.549	1.333	.00266
39.75	.267	14.87	5.96	.0618	.0823	.539	1.332	.00262
39.75	.288	14.89	6.36	.0607	.0811	.542	1.336	.00260
39.75	.310	14.90	6.78	.0604	.0801	.527	1.326	.00258
39.75	.151	28.72	6.74	.0596	.0790	.530	1.326	.00269
39.75	.187	29.03	8.31	.0583	.0764	.516	1.310	.00252
39.75	.217	29.26	9.56	.0566	.0753	.509	1.330	.00248
39.75	.244	29.75	10.68	.0561	.0729	.503	1.300	.00245
39.75	.290	30.35	12.53	.0547	.0715	.489	1.307	.00240
39.75	.311	30.55	13.45	.0542	.0705	.498	1.301	.00238
39.75	.107	73.39	12.25	.0538	.0708	.488	1.316	.00241
38.75	.152	74.57	17.34	.0516	.0667	.483	1.293	.00231
39.75	.187	75.87	21.29	.0495	.0638	.473	1.289	.00226
39.75	.221	78.80	25.82	.0497	.0637	.483	1.282	.00221
39.75	.235	78.34	26.21	.0497	.0639	.483	1.286	.00221
39.75	.247	78.22	28.11	.0492	.0625	.476	1.270	.00219
39.75	.260	79.82	28.86	.0483	.0616	.470	1.275	.00218
39.75	.272	80.51	30.29	.0488	.0615	.469	1.260	.00217
51.75	.317	7.97	4.78	.0887	.1200	.743	1.353	
51.75	0.221	14.84	6.48	0.0802	0.1067	0.693	1.330	
51.75	.248	14.89	7.16	.0781	.1047	.689	1.341	
51.75	.274	14.90	7.92	.0774	.1018	.676	1.319	
51.75	.295	15.13	8.52	.0751	.1001	.665	1.333	
51.75	.317	15.20	9.05	.0751	.1000	.669	1.332	...
51.75	.155	29.66	8.96	.0734	.0972	.655	1.324	
51.75	.190	29.81	10.95	.0723	.0954	.655	1.320	0.00255
51.75	.221	30.00	12.55	.0704	.0925	.643	1.314	.00250
51.75	.249	29.66	14.09	.0698	.0909	.636	1.302	.00246
51.75	.273	29.56	15.53	.0689	.0893	.643	1.296	.00242
51.75	.295	29.76	16.61	.0677	.0884	.629	1.306	.00239
51.75	.319	28.47	16.94	.0688	.0885	.633	1.286	.00238
51.75	.110	78.89	18.89	.0676	.0871	.633	1.288	.00234
51.75	.157	85.15	26.75	.0630	.0808	.611	1.283	.00222
51.75	.193	80.49	30.55	.0622	.0791	.595	1.272	.00219
51.75	.224	76.25	32.54	.0633	.0807	.609	1.275	.00217
51.75	.238	78.02	34.78	.0634	.0802	.609	1.267	.00215
51.75	.251	80.29	36.82	.0629	.0791	.603	1.258	.00214
51.75	.263	81.69	39.32	.0625	.0792	.603	1.267	.00212
51.75	.275	80.84	41.24	.0606	.0771	.599	1.272	.00210

TABLE IV.—COMPUTED FRICTIONAL RESISTANCE LAW

C_f	P_x	C_F	P_δ	$\dfrac{\delta^*}{\theta}$
0.0015	7.314×10^8	0.00169	616450.	1.216
.0016	3.918	.00183	359220.	1.224
.0017	2.279	.00193	219360.	1.233
.0018	1.366	.00205	139670.	1.241
.0019	8.513×10^7	.00216	92100.	1.249
.0020	5.487	.00229	62700.	1.257
.0021	3.636	.00241	43852.	1.266
.0022	2.481	.00253	31412.	1.274
.0023	1.734	.00266	23023.	1.281
.0024	1.239	.00278	17196.	1.289
.0025	8.995×10^6	.00290	13053.	1.297
.0026	6.662	.00303	10086.	1.305
.0027	5.020	.00315	7901.	1.312
.0028	3.826	.00327	6265.	1.320
.0029	2.955	.00340	5028.	1.327
.0030	2.314	.00353	4083.	1.334
.0031	1.830	.00365	3343.	1.342
.0032	1.463	.00378	2766.	1.350
.0033	1.182	.00390	2308.	1.357
				1.364
.0034	9.621×10^5	.00403	1941.	1.371
.0035	7.913	.00416	1645.	
.0036	6.535	.00429	1401.	1.378
.0037	5.444	.00442	1203.	1.386
.0038	4.561	.00455	1038.	1.393
.0039	3.853	.00468	901.4	1.401
.0040	3.273	.00481	787.2	1.407
.0041	2.794	.00494	680.5	1.415
.0042	2.401	.00506	607.4	1.422
.0043	2.069	.00520	537.5	1.429
.0044	1.795	.00532	477.3	1.436
.0045	1.560	.00546	426.0	1.443